

TUM-HEP-496/02

MPI-PhT/2002-80

December 2002

The Impact of Universal Extra Dimensions on the Unitarity Triangle and Rare K and B Decays

Andrzej J. Buras^a, Michael Spranger^{a,b} and Andreas Weiler^a

^a *Physik Department, Technische Universität München
D-85748 Garching, Germany*

^b *Max-Planck-Institut für Physik - Werner-Heisenberg-Institut
D-80805 München, Germany*

Abstract

We calculate the contributions of the Kaluza-Klein (KK) modes to the $K_L - K_S$ mass difference ΔM_K , the parameter ε_K , the $B_{d,s}^0 - \bar{B}_{d,s}^0$ mixing mass differences $\Delta M_{d,s}$ and rare decays $K^+ \rightarrow \pi^+ \nu \bar{\nu}$, $K_L \rightarrow \pi^0 \nu \bar{\nu}$, $K_L \rightarrow \mu^+ \mu^-$, $B \rightarrow X_{s,d} \nu \bar{\nu}$ and $B_{s,d} \rightarrow \mu \bar{\mu}$ in the Appelquist, Cheng and Dobrescu (ACD) model with one universal extra dimension. For the compactification scale $1/R = 200$ GeV the KK effects in these processes are governed by a 17% enhancement of the $\Delta F = 2$ box diagram function $S(x_t, 1/R)$ and by a 37% enhancement of the Z^0 penguin diagram function $C(x_t/1/R)$ relative to their Standard Model (SM) values. This implies the suppressions of $|V_{td}|$ by 8%, of $\bar{\eta}$ by 11% and of the angle γ in the unitarity triangle by 10°. ΔM_s is increased by 17%. ΔM_K is essentially unaffected. All branching ratios considered in this paper are increased with a hierarchical structure of enhancements: $K^+ \rightarrow \pi^+ \nu \bar{\nu}$ (16%), $K_L \rightarrow \pi^0 \nu \bar{\nu}$ (17%), $B \rightarrow X_d \nu \bar{\nu}$ (22%), $(K_L \rightarrow \mu \bar{\mu})_{\text{SD}}$ (38%), $B \rightarrow X_s \nu \bar{\nu}$ (44%), $B_d \rightarrow \mu \bar{\mu}$ (46%) and $B_s \rightarrow \mu \bar{\mu}$ (72%). For $1/R = 250$ (300) GeV all these effects are decreased roughly by a factor of 1.5 (2.0). We emphasize that the GIM mechanism assures the convergence of the sum over the KK modes in the case of Z^0 penguin diagrams and we give the relevant Feynman rules for the five dimensional ACD model. We also emphasize that a consistent calculation of branching ratios has to take into account the modifications in the values of the CKM parameters.

1 Introduction

During the last years there has been an increased interest in models with extra dimensions. Among them a special role play the ones with universal extra dimensions (UED). In these models all the Standard Model (SM) fields are allowed to propagate in all available dimensions. Above the compactification scale $1/R$ a given UED model becomes a higher dimensional field theory whose equivalent description in four dimensions consists of the SM fields, the towers of their Kaluza-Klein (KK) partners and additional towers of KK modes that do not correspond to any field in the SM. The simplest model of this type is the Appelquist, Cheng and Dobrescu (ACD) model [1] with one extra universal dimension. In this model the only additional free parameter relative to the SM is the compactification scale $1/R$. Thus all the masses of the KK particles and their interactions among themselves and with the SM particles are described in terms of $1/R$ and the parameters of the SM. This economy in new parameters should be contrasted with supersymmetric theories and models with an extended Higgs sector.

A very important property of the ACD model is the conservation of KK parity that implies the absence of tree level KK contributions to low energy processes taking place at scales $\mu \ll 1/R$. In this context the flavour changing neutral current (FCNC) processes like particle-antiparticle mixing and rare K and B decays are of particular interest. As these processes appearing in the SM first at one-loop are strongly suppressed, the one-loop contributions from the KK modes to them could in principle be important.

The effects of the KK modes on various processes of interest have been investigated in a number of papers. In [1] their impact on the precision electroweak observables assuming a light Higgs ($m_H \leq 250$ GeV) led to the lower bound $1/R \geq 300$ GeV. Subsequent analyses of the decay $B \rightarrow X_s \gamma$ [2] and of the anomalous magnetic moment [3] have shown the consistency of the ACD model with the data for $1/R \geq 300$ GeV. The scale of $1/R$ as low as 300 GeV would lead to an exciting phenomenology in the next generation of colliders [4, 5, 6, 7]. Moreover the cosmic relic density of the lightest KK particle as a dark matter candidate turned out to be of the right order of magnitude [8]. The related experimental signatures have been investigated in ref. [9].

Very recently Appelquist and Yee [10] have extended the analysis of [1] by considering a heavy Higgs ($m_H \geq 250$ GeV). It turns out that in this case the lower bound on $1/R$ can be decreased to 250 GeV, implying larger KK contributions to various low energy processes, in particular to the FCNC processes. Among the latter only the decay $B \rightarrow X_s \gamma$ has been investigated within the ACD model so far [2] and it is desirable to consider other FCNC processes.

In the present paper we calculate for the first time the $B_{d,s}^0 - \bar{B}_{d,s}^0$ mixing mass differences $\Delta M_{d,s}$, the $K_L - K_S$ mass difference, the CP violation parameter ε_K and the branching ratios

for the rare decays $K^+ \rightarrow \pi^+ \nu \bar{\nu}$, $K_L \rightarrow \pi^0 \nu \bar{\nu}$, $K_L \rightarrow \mu^+ \mu^-$, $B \rightarrow X_{s,d} \nu \bar{\nu}$ and $B_{s,d} \rightarrow \mu \bar{\mu}$ in the ACD model with one universal extra dimension. In the forthcoming paper [11] we will analyze the decays $B \rightarrow X_s \gamma$, $B \rightarrow X_s l^+ l^-$ and $K_L \rightarrow \pi^0 e^+ e^-$. In order to be more general we will include the results for $1/R = 200 \text{ GeV}$ that is only slightly below the lowest value of $1/R = 250 \text{ GeV}$ allowed by the electroweak precision data.

As our analysis shows, the ACD model with one extra dimension has a number of interesting properties from the point of view of FCNC processes discussed here. These are:

- GIM mechanism [12] that improves significantly the convergence of the sum over the KK modes corresponding to the top quark, removing simultaneously to an excellent accuracy the contributions of the KK modes corresponding to lighter quarks and leptons. This feature removes the sensitivity of the calculated branching ratios to the scale $M_s \gg 1/R$ at which the higher dimensional theory becomes non-perturbative and at which the towers of the KK particles must be cut off in an appropriate way. This should be contrasted with models with fermions localized on the brane, in which the KK parity is not conserved and the sum over the KK modes diverges. In these models the results are sensitive to M_s and the KK effects in $\Delta M_{s,d}$ are significantly larger [13] than found here.
- The low energy effective Hamiltonians are governed by local operators already present in the SM. As flavour violation and CP violation in this model is entirely governed by the CKM matrix, the ACD model belongs to the class of the so-called models with minimal flavour violation (MFV) as defined in [14]. This has automatically two important consequences.
 - The impact of the KK modes on the processes discussed here amounts to the modification of the Inami-Lim one-loop functions [15]. This is the function S [16] in the case of $\Delta M_{d,s}$ and of the parameter ε_K and the functions X and Y [17] in the case of the rare decays considered. In the ACD model these three functions depend only on m_t and the single new parameter, the compactification radius R .
 - The unitarity triangle constructed from $|V_{ub}/V_{cb}|$, $\Delta M_d/\Delta M_s$ and the $\sin 2\beta$ extracted from the CP asymmetry $a_{\psi K_S}$ is common to the SM model and the ACD model. That is, the R -dependence drops out in this construction. Which of these two models, if any, is consistent with the data can only be found out by analyzing ΔM_d and ΔM_s separately, ε_K and in particular the branching ratios for rare K and B decays that depend explicitly on R .

Our paper is organized as follows. In section 2, we summarize those ingredients of the ACD

model that are relevant for our analysis. In particular, we give in appendix A the set of the relevant Feynman rules in the ACD model that have not been given so far in the literature. In section 3, we calculate the KK contributions to the box diagram function S and we discuss the implications of these contributions for ΔM_K , ΔM_d , ΔM_s , ε_K and the unitarity triangle. In section 4, we calculate the corresponding corrections to the functions X and Y that receive the dominant contribution from Z^0 -penguins and we analyze the implications of these corrections for the rare decays $K^+ \rightarrow \pi^+ \nu \bar{\nu}$, $K_L \rightarrow \pi^0 \nu \bar{\nu}$, $K_L \rightarrow \mu^+ \mu^-$, $B \rightarrow X_{s,d} \nu \bar{\nu}$ and $B_{s,d} \rightarrow \mu \bar{\mu}$. In section 5, we summarize our results and give a brief outlook.

Very recently an analysis of $\Delta M_{s,d}$ in the ACD model has been presented in [18]. The result for the function S found by these authors differs significantly from our result with the effect of the KK modes being by roughly a factor of three larger than what we find. As the authors do not present the details of their calculation, it is impossible to identify the origin of this discrepancy.

2 The Five Dimensional ACD Model

The five dimensional UED model introduced by Appelquist, Cheng and Dobrescu (ACD) in [1] uses orbifold compactification to produce chiral fermions in 4 dimensions. This is not the case in the models described in [19], where all fermions are localized on the 4 dimensional brane. However, there are many similarities between these two classes of models, and some of the issues discussed in this section have already been presented in detail in [19]. We also rely on [1, 20, 21].

2.1 Kaluza-Klein mode expansion

The topology of the fifth dimension is the orbifold S^1/Z_2 , and the coordinate $y \equiv x^5$ runs from 0 to $2\pi R$, where R is the compactification radius. The orbifold has two fixed points, $y = 0$ and $y = \pi R$. The boundary conditions given at these fixed points determine the Kaluza-Klein (KK) mode expansion of the fields.

A scalar field ϕ has to be either even or odd under the transformation $\mathbf{P}_5 : y \rightarrow -y$, and therefore

$$\left. \begin{array}{ll} \partial_5 \phi^+ = 0 & \text{for even fields} \\ \phi^- = 0 & \text{for odd fields} \end{array} \right\} \quad \text{at } y = 0, \pi R. \quad (2.1)$$

These are von Neumann and Dirichlet boundary conditions respectively at the fixed points. The

associated KK expansions are

$$\begin{aligned}\phi^+(x, y) &= \frac{1}{\sqrt{2\pi R}}\phi_{(0)}^+(x) + \frac{1}{\sqrt{\pi R}}\sum_{n=1}^{\infty}\phi_{(n)}^+(x)\cos\frac{ny}{R}, \\ \phi^-(x, y) &= \frac{1}{\sqrt{\pi R}}\sum_{n=1}^{\infty}\phi_{(n)}^-(x)\sin\frac{ny}{R},\end{aligned}\tag{2.2}$$

where $x \equiv x^\mu$, $\mu = 0, 1, 2, 3$, denotes the four non-compact space-time coordinates. The fields $\phi_{(n)}^\pm(x)$ are called Kaluza-Klein modes.

A vector field A^M in 5 dimensions has five components, $M = 0, 1, 2, 3, 5$. The orbifold compactification forces the first four components to be even under \mathbf{P}_5 , while the fifth component is odd:

$$\left.\begin{array}{l}\partial_5 A^\mu = 0 \\ A^5 = 0\end{array}\right\} \text{ at } y = 0, \pi R.\tag{2.3}$$

Hence, the KK expansion of a vector field is

$$\begin{aligned}A^\mu(x, y) &= \frac{1}{\sqrt{2\pi R}}A_{(0)}^\mu(x) + \frac{1}{\sqrt{\pi R}}\sum_{n=1}^{\infty}A_{(n)}^\mu(x)\cos\frac{ny}{R}, \\ A^5(x, y) &= \frac{1}{\sqrt{\pi R}}\sum_{n=1}^{\infty}A_{(n)}^5(x)\sin\frac{ny}{R}.\end{aligned}\tag{2.4}$$

A Dirac spinor ψ in 5 dimensions is a four component object. Using the chirality projectors $P_{R/L} = (1 \pm \gamma_5)/2$, a spinor $\psi = (P_R + P_L)\psi = \psi_R + \psi_L$ has to satisfy either

$$\left.\begin{array}{l}\partial_5\psi_R^+ = 0 \\ \psi_L^+ = 0\end{array}\right\} \text{ at } y = 0, \pi R \quad \text{or} \quad \left.\begin{array}{l}\partial_5\psi_L^- = 0 \\ \psi_R^- = 0\end{array}\right\} \text{ at } y = 0, \pi R.\tag{2.5}$$

The respective KK mode expansions are

$$\begin{aligned}\psi^+(x, y) &= \frac{1}{\sqrt{2\pi R}}\psi_{R(0)}(x) + \frac{1}{\sqrt{\pi R}}\sum_{n=1}^{\infty}\left(\psi_{R(n)}(x)\cos\frac{ny}{R} + \psi_{L(n)}(x)\sin\frac{ny}{R}\right), \\ \psi^-(x, y) &= \frac{1}{\sqrt{2\pi R}}\psi_{L(0)}(x) + \frac{1}{\sqrt{\pi R}}\sum_{n=1}^{\infty}\left(\psi_{L(n)}(x)\cos\frac{ny}{R} + \psi_{R(n)}(x)\sin\frac{ny}{R}\right).\end{aligned}\tag{2.6}$$

The zero-mode is either right-handed or left-handed. The non-zero-modes come in chiral pairs. This chirality structure is a natural consequence of the orbifold boundary conditions.

We can derive Feynman rules for the KK modes by explicitly integrating over the fifth dimension in the action:

$$S = \int d^4x \int_0^{2\pi R} dy \mathcal{L}_5 = \int d^4x \mathcal{L}_4.\tag{2.7}$$

Using the KK mode expansions in (2.2), (2.4) and (2.6), the five dimensional Lagrangian \mathcal{L}_5 reduces to the four dimensional Lagrangian \mathcal{L}_4 which contains all KK modes. The field content is arranged such that the zero-modes are the 4 dimensional SM particles, whereas the higher modes constitute their KK excitations. Moreover there are additional KK modes that do not correspond to any field in the SM.

2.2 Universal Extra Dimensions

In the UED scenarios, all fields present in the Standard Model live in the extra dimensions, i.e. they are functions of all space-time coordinates.

For bosonic fields, one simply replaces all derivatives and fields in the SM Lagrangian by their 5 dimensional counterparts. There are the $U(1)_Y$ gauge field B and the $SU(2)_L$ gauge field A^a , as well as the $SU(3)_C$ QCD gauge fields. The Higgs doublet is

$$\phi = \frac{1}{\sqrt{2}} \begin{pmatrix} \chi^2 + i\chi^1 \\ \psi - i\chi^3 \end{pmatrix} = \begin{pmatrix} i\chi^+ \\ \frac{1}{\sqrt{2}}(\psi - i\chi^3) \end{pmatrix}, \quad (2.8)$$

where

$$\chi^\pm = \frac{1}{\sqrt{2}} [\chi^1 \mp i\chi^2]. \quad (2.9)$$

It is chosen to be even under \mathbf{P}_5 so it possesses a zero-mode. By assigning a vacuum expectation value to that zero-mode with the substitution $\psi \rightarrow \hat{v} + H$, we can give masses to the fermions. Note that we label all parameters of the 5 dimensional Lagrangian with a caret. It is convenient to introduce 4 dimensional parameters that are related to their 5 dimensional counterparts by factors of $\sqrt{2\pi R}$, see appendix A.

Fermions living in five dimensions are more involved. In order to write down a Lorentz invariant Lagrangian, we need one Γ -matrix for each space-time dimension to satisfy the Clifford algebra

$$\{\Gamma^M, \Gamma^N\} = 2g^{MN}, \quad M, N = 0, 1, 2, 3, 5. \quad (2.10)$$

The metric $g^{MN} = \text{diag}(1, -1, -1, -1, -1)$ is the natural extension of the flat Minkowskian metric for one extra space dimension. For the Γ -matrices, we take

$$\begin{aligned} \Gamma^\mu &= \gamma^\mu, \quad \mu = 0, 1, 2, 3 \\ \Gamma^5 &= i\gamma_5, \end{aligned} \quad (2.11)$$

with $\gamma_5 = i\gamma^0\gamma^1\gamma^2\gamma^3$. The 5 dimensional kinetic Lagrangian for spinor fields can now be written as [20]

$$\mathcal{L}_5 = i\bar{\psi}\Gamma^M\partial_M\psi = \bar{\psi}(i\partial\!\!\!/ - \gamma_5\partial_5)\psi. \quad (2.12)$$

Integrating over the fifth dimension yields

$$\mathcal{L}_4 = \int_0^{2\pi R} dy \mathcal{L}_5 = \sum_{n=0}^{\infty} \bar{\psi}_{(n)}^{\pm} \left(i\partial_5 \pm \frac{n}{R} \right) \psi_{(n)}^{\pm}, \quad (2.13)$$

where the sign of the KK mass term n/R depends on the choice in (2.5).

Note that the zero-mode remains massless unless we apply the Higgs mechanism. Note also that all fields in the 4 dimensional Lagrangian receive the KK mass n/R on account of the derivative operator ∂_5 acting on them. These tree-level masses are shifted by radiative corrections due to gauge interactions and boundary terms localized at the fixed points [22]. Since these corrections are a two-loop effect on the processes considered, we will use the tree-level mass relations in our calculations.

2.3 Gauge fixing and Goldstone mixing

In the 5 dimensional ACD model, we can use the same gauge fixing procedure as in models in which the fermions are localized on the 4 dimensional subspace. We adopt the various gauge fixing functionals given in [19] and adapt them to the case of the SM gauge group $U(1)_Y \times SU(2)_L$ with one Higgs doublet:

$$\begin{aligned} \mathcal{G}_B[B^\mu, B_5, \chi^3] &= \frac{1}{\sqrt{\xi}} \left[\partial_\mu B^\mu - \xi \left(\frac{\hat{g}'}{2} \hat{v} \chi^3 + \partial_5 B_5 \right) \right], \\ \mathcal{G}_A^a[A^{a\mu}, A_5^a, \chi^a] &= \frac{1}{\sqrt{\xi}} \left[\partial_\mu A^{a\mu} - \xi \left(-\frac{\hat{g}_2}{2} \hat{v} \chi^a + \partial_5 A_5^a \right) \right], \end{aligned} \quad (2.14)$$

where \hat{g}' and \hat{g}_2 are the respective 5 dimensional $U(1)_Y$ and $SU(2)_L$ gauge coupling constants. This is a natural extension of the 4 dimensional R_ξ -gauge fixing.

With the gauge fixed, we can diagonalize the kinetic terms of the bosons and finally derive expressions for the propagators. Compared to the SM, there are the additional KK mass terms. As they are common to all fields, their contribution to the gauge boson mass matrix is proportional to the unity matrix. As a consequence, the electroweak mixing angle θ_w is the same for all KK modes, and we have

$$\begin{pmatrix} Z^M \\ A^M \end{pmatrix} = \begin{pmatrix} \cos \theta_w & -\sin \theta_w \\ \sin \theta_w & \cos \theta_w \end{pmatrix} \begin{pmatrix} A^{3M} \\ B^M \end{pmatrix}, \quad (2.15)$$

$$W^{\pm M} = \frac{1}{\sqrt{2}} (A^{1M} \mp i A^{2M}), \quad (2.16)$$

where

$$s_w \equiv \sin \theta_w = \frac{g'}{\sqrt{g_2^2 + g'^2}} \quad \text{and} \quad c_w \equiv \cos \theta_w = \frac{g_2}{\sqrt{g_2^2 + g'^2}}. \quad (2.17)$$

For the μ -components, (2.15) and (2.16) already give the mass eigenstates

$$\begin{aligned} Z_{(n)}^\mu &= c_w A_{(n)}^{3\mu} - s_w B_{(n)}^\mu, \\ A_{(n)}^\mu &= s_w A_{(n)}^{3\mu} + c_w B_{(n)}^\mu, \\ W_{(n)}^{\pm\mu} &= \frac{1}{\sqrt{2}} \left(A_{(n)}^{1\mu} \mp i A_{(n)}^{2\mu} \right). \end{aligned} \quad (2.18)$$

The zero-modes $Z_{(0)}^\mu$ and $W_{(0)}^{\pm\mu}$ have the masses

$$M_Z = \frac{v}{2} \sqrt{g_2^2 + g'^2} \quad \text{and} \quad M_W = \frac{v}{2} g_2. \quad (2.19)$$

The components $Z_{5(n)}$ and $W_{5(n)}^\pm$ mix with the Higgs modes $\chi_{(n)}^a$, while $A_{5(n)}$ as defined in (2.15) is a mass eigenstate.

Because of the KK contribution to the mass matrix, the Higgs components χ^\pm and χ^3 with $n \neq 0$ no longer play the role of Goldstone bosons. Instead, they mix with W_5^\pm and Z_5 to form, in addition to the Goldstone modes $G_{(n)}^0$ and $G_{(n)}^\pm$, three additional *physical* scalar modes $a_{(n)}^0$ and $a_{(n)}^\pm$. The former allow the gauge bosons to acquire masses without breaking gauge invariance. The propagator terms are diagonalized by the orthogonal transformations

$$G_{(n)}^0 = \frac{1}{M_{Z(n)}} \left[M_Z \chi_{(n)}^3 - \frac{n}{R} Z_{5(n)} \right], \quad a_{(n)}^0 = \frac{1}{M_{Z(n)}} \left[\frac{n}{R} \chi_{(n)}^3 + M_Z Z_{5(n)} \right], \quad (2.20)$$

$$G_{(n)}^\pm = \frac{1}{M_{W(n)}} \left[M_W \chi_{(n)}^\pm - \frac{n}{R} W_{5(n)}^\pm \right], \quad a_{(n)}^\pm = \frac{1}{M_{W(n)}} \left[\frac{n}{R} \chi_{(n)}^\pm + M_W W_{5(n)}^\pm \right] \quad (2.21)$$

with $M_{Z(n)}$ and $M_{W(n)}$ given in (A.2).

For the zero-modes, we can identify $\chi_{(0)}^3$ and $\chi_{(0)}^\pm$ as the Goldstone bosons that give masses to $Z_{(0)}^\mu$ and $W_{(0)}^{\pm\mu}$. With increasing n , the contributions of $Z_{5(n)}$ and $W_{5(n)}^\pm$ dominate the Goldstone modes, while $\chi_{(n)}^3$ and $\chi_{(n)}^\pm$ provide the main fraction of $a_{(n)}^0$ and $a_{(n)}^\pm$. The physical Higgs $H_{(n)}$ does not mix with $A_{5(n)}$. The latter constitutes an additional *unphysical* scalar mode which turns out to be the Goldstone mode for $A_{(n)}^\mu$ for $n \geq 1$.

Note that the fields a^0 , a^\pm and A_5 do not have zero modes. Consequently, the photon $A_{(0)}^\mu$ remains massless.

2.4 Fermion-Higgs coupling

The Yukawa coupling of the Higgs doublet to the quark fields is a pivotal part of the Lagrangian concerning chirality. Analogous to the SM, we write

$$\mathcal{L}_{qH}(x, y) = \overline{\mathcal{Q}}' \hat{\lambda}_D \mathcal{D}' \phi + \overline{\mathcal{Q}}' \hat{\lambda}_U \mathcal{U}' i \sigma^2 \phi^* + \text{h.c.} \quad (2.22)$$

with the three generation gauge eigenstates

$$\mathcal{Q}' = \left(\left(\begin{array}{c} \mathcal{Q}'_u \\ \mathcal{Q}'_d \end{array} \right), \left(\begin{array}{c} \mathcal{Q}'_c \\ \mathcal{Q}'_s \end{array} \right), \left(\begin{array}{c} \mathcal{Q}'_t \\ \mathcal{Q}'_b \end{array} \right) \right)^T, \quad (2.23)$$

$$\mathcal{U}' = \left(\begin{array}{c} \mathcal{U}'_u \\ \mathcal{U}'_c \\ \mathcal{U}'_t \end{array} \right), \quad \mathcal{D}' = \left(\begin{array}{c} \mathcal{D}'_d \\ \mathcal{D}'_s \\ \mathcal{D}'_b \end{array} \right). \quad (2.24)$$

The $SU(2)$ doublets \mathcal{Q}' are odd under \mathbf{P}_5 , while the singlets \mathcal{U}' and \mathcal{D}' are even. Due to this assignment, the zero-modes have the same chirality as the quark fields in the SM.

The fermions receive masses both through spontaneous symmetry breaking and the KK expansion as described in section 2.2. In order to diagonalize the Yukawa couplings between fermions of equal charge, we apply the biunitary transformation

$$\mathcal{Q}'_{\mathcal{U}} = S_{\mathcal{U}} \mathcal{Q}''_{\mathcal{U}}, \quad \mathcal{Q}'_{\mathcal{D}} = S_{\mathcal{D}} \mathcal{Q}''_{\mathcal{D}}, \quad (2.25)$$

$$\mathcal{U}' = T_{\mathcal{U}} \mathcal{U}'', \quad \mathcal{D}' = T_{\mathcal{D}} \mathcal{D}'', \quad (2.26)$$

so that the resulting mass matrices

$$M_{\mathcal{U}} = -\frac{v}{\sqrt{2}} S_{\mathcal{U}}^\dagger \lambda_{\mathcal{U}} T_{\mathcal{U}}, \quad M_{\mathcal{D}} = -\frac{v}{\sqrt{2}} S_{\mathcal{D}}^\dagger \lambda_{\mathcal{D}} T_{\mathcal{D}} \quad (2.27)$$

are diagonal and their eigenvalues (m_u, m_c, m_t) and (m_d, m_s, m_b) are non-negative. This step is analogous to the SM and leads to the CKM matrix $V_{\text{CKM}} = S_{\mathcal{U}}^\dagger S_{\mathcal{D}}$ which is unique for all KK levels. Next we apply to each flavour $f = u, c, t, d, s, b$ the unitary transformation

$$\left(\begin{array}{c} \mathcal{U}''_{f(n)} \\ \mathcal{Q}''_{f(n)} \end{array} \right) = \left(\begin{array}{cc} -\gamma_5 \cos \alpha_{f(n)} & \sin \alpha_{f(n)} \\ \gamma_5 \sin \alpha_{f(n)} & \cos \alpha_{f(n)} \end{array} \right) \left(\begin{array}{c} \mathcal{U}_{f(n)} \\ \mathcal{Q}_{f(n)} \end{array} \right) \quad (2.28)$$

and the same expression with \mathcal{U} replaced by \mathcal{D} for the down-type quarks. The mixing angle is

$$\tan 2\alpha_{f(n)} = \frac{m_f}{n/R} \quad \text{for } n \geq 1. \quad (2.29)$$

In (2.28) we have used γ_5 to get both eigenvalues positive and equal to

$$m_{f(n)} = \sqrt{\frac{n^2}{R^2} + m_f^2}. \quad (2.30)$$

In phenomenological applications we have $n/R \geq 200$ GeV and can therefore set all mixing angles to zero except for the top quark.

The Yukawa coupling of the leptons to the Higgs doublet is similar to that of the quarks. The lepton doublets take the form

$$\mathcal{L}' = \left(\left(\begin{array}{c} \mathcal{L}'_{\nu_e} \\ \mathcal{L}'_e \end{array} \right), \left(\begin{array}{c} \mathcal{L}'_{\nu_\mu} \\ \mathcal{L}'_\mu \end{array} \right), \left(\begin{array}{c} \mathcal{L}'_{\nu_\tau} \\ \mathcal{L}'_\tau \end{array} \right) \right)^T, \quad (2.31)$$

and the singlets are

$$\mathcal{E}' = \left(\begin{array}{c} \mathcal{E}'_e \\ \mathcal{E}'_\mu \\ \mathcal{E}'_\tau \end{array} \right). \quad (2.32)$$

Due to their smallness, we can ignore neutrino masses in heavy flavour physics. Hence, the neutrino singlets do not couple to the other particles and are therefore omitted. Due to their small Yukawa masses, we can set the mixing angles for all KK excitations of the leptons to zero. The lepton masses are given by Eq. (2.30).

The Feynman rules can be found in appendix A.

3 $B_{d,s}^0 - \bar{B}_{d,s}^0$ Mixing and ε_K

3.1 $B_{d,s}^0 - \bar{B}_{d,s}^0$ Mixing

The effective Hamiltonian for $\Delta B = 2$ transitions in the SM [23] can be generalized to the ACD model as follows

$$\begin{aligned} \mathcal{H}_{\text{eff}}^{\Delta B=2} = & \frac{G_F^2}{16\pi^2} M_W^2 (V_{tb}^* V_{tq})^2 \eta_B S(x_t, 1/R) \times \\ & \times \left[\alpha_s^{(5)}(\mu_b) \right]^{-6/23} \left[1 + \frac{\alpha_s^{(5)}(\mu_b)}{4\pi} J_5 \right] Q(\Delta B = 2) + h.c. \end{aligned} \quad (3.1)$$

Here $\mu_b = \mathcal{O}(m_b)$, $J_5 = 1.627$,

$$Q(\Delta B = 2) = (\bar{b}q)_{V-A}(\bar{b}q)_{V-A}, \quad q = d, s \quad (3.2)$$

with $(\bar{b}q)_{V-A} \equiv \bar{b}\gamma_\mu(1 - \gamma_5)q$ and [23, 24]

$$\eta_B = 0.55 \pm 0.01 \quad (3.3)$$

describes the short distance QCD corrections to which we will return below.

The function $S(x_t, 1/R)$ is given as follows

$$S(x_t, 1/R) = S_0(x_t) + \sum_{n=1}^{\infty} S_n(x_t, x_n) \quad (3.4)$$

where

$$x_t = \frac{m_t^2}{M_W^2}, \quad x_n = \frac{m_n^2}{M_W^2}, \quad m_n = \frac{n}{R} \quad (3.5)$$

and

$$S_0(x_t) = \frac{4x_t - 11x_t^2 + x_t^3}{4(1-x_t)^2} - \frac{3x_t^3 \ln x_t}{2(1-x_t)^3} \quad (3.6)$$

results from the usual box diagrams with (W^\pm, t) and (G^\pm, t) exchanges with the m_t independent terms removed by the GIM mechanism.

The KK contributions are represented by the functions $S_n(x_t, x_n)$ that are obtained by calculating the box diagrams in fig. 1 with $W_{(n)}^\pm, a_{(n)}^\pm, G_{(n)}^\pm, \mathcal{Q}_{i(n)}$ and $\mathcal{U}_{i(n)}$ ($i = u, c, t$) exchanges and multiplying the result by $i/4$, where $1/4$ is a combinatorial factor. We neglect momenta and masses of external quarks. Denoting the contribution of the sum of the diagrams corresponding to a given pair $(m_{i(n)}, m_{j(n)})$ to $S_n(x_t, x_n)$ by $F(x_{i(n)}, x_{j(n)})$ with

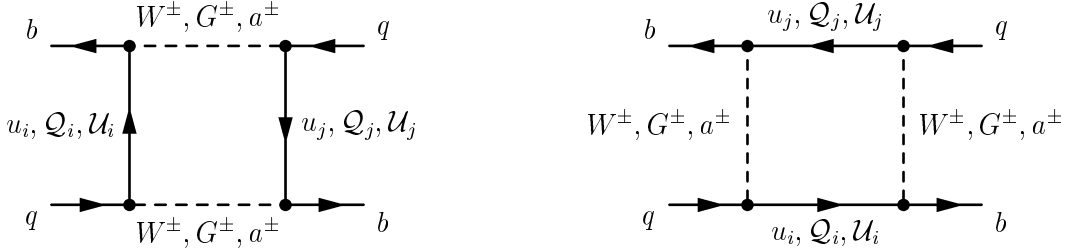


Figure 1: Box diagrams contributing to $S_n(x_t, x_n)$. We suppress the KK mode number.

$$x_{i(n)} = \frac{m_{i(n)}^2}{M_{W(n)}^2} \quad (3.7)$$

and $m_{i(n)}$ and $M_{W(n)}$ defined in (2.30) and (A.2), and using the unitarity of the CKM matrix, we have

$$S_n(x_t, x_n) \equiv F(x_{t(n)}, x_{t(n)}) + F(x_{u(n)}, x_{u(n)}) - 2F(x_{t(n)}, x_{u(n)}). \quad (3.8)$$

As with increasing n the modes $\mathcal{Q}_{t(n)}, \mathcal{U}_{t(n)}, \mathcal{Q}_{u(n)}$ and $\mathcal{U}_{u(n)}$ become increasingly degenerate in mass and

$$x_{t(n)} \rightarrow x_{u(n)} \rightarrow 1, \quad (3.9)$$

the functions $S_n(x_t, x_n)$ decrease with increasing n so that only a few terms in the sum in (3.4) are relevant. This is seen in fig. 2 (a) where we show $S_n(x_t, x_n)$ as a function of n/R . We will discuss this in more detail in section 4.8.

The contributions from different sets of diagrams to the functions $F(x_{i(n)}, x_{j(n)})$ are collected in appendix B. It turns out that the contribution from the pair $(a_{(n)}^\pm, a_{(n)}^\pm)$ is by far dominant. We illustrate this in fig. 2 (a). In phenomenological applications it is more useful to work with the variables x_t and x_n than with $x_{i(n)}$. We find

$$S_n(x_t, x_n) = \frac{1}{4(x_t - 1)^3 x_t} \left[6x_n x_t - 5x_t^2 - 12x_n x_t^2 + 15x_t^3 + 10x_n x_t^3 - 11x_t^4 - 4x_n x_t^4 + x_t^5 - 2x_n(x_t - 1)^3(3x_n + 3x_n x_t - x_t) \ln \frac{x_n}{1 + x_n} + \left(-6x_n^2 + 2x_n x_t + 12x_n^2 x_t - 6x_n x_t^2 - 2x_t^3 + 14x_n x_t^3 - 2x_n^2 x_t^3 + 6x_t^4 - 2x_n x_t^4 \right) \ln \frac{x_t + x_n}{1 + x_n} \right]. \quad (3.10)$$

In fig. 2 (b) we plot $S(x_t, 1/R)$ versus $1/R$. For $1/R = 200$ GeV we observe a 17% enhancement of the function S with respect to its SM value given by $S_0(x_t)$. For $1/R = 250$ GeV this enhancement decreases to 11% and it is only 4% for $1/R = 400$ GeV.

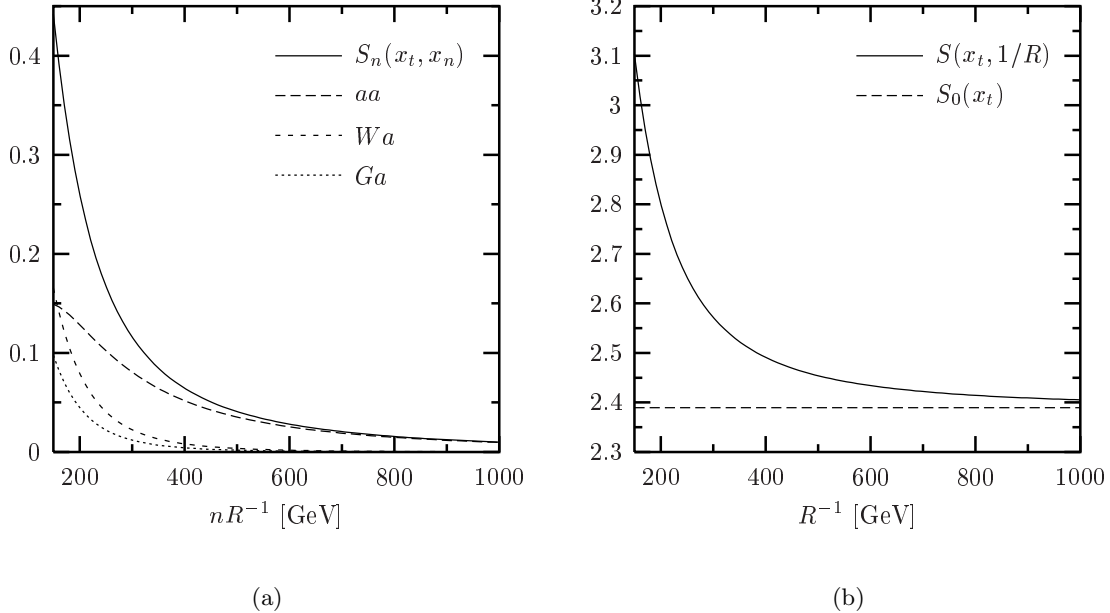


Figure 2: (a) Contribution S_n of the n^{th} KK mode to $S(x_t, 1/R)$. The contributions with a^\pm dominate, those with only G^\pm and W^\pm are negligible and not shown. (b) The functions $S(x_t, 1/R)$ and $S_0(x_t)$.

Proceeding as in the SM, we can calculate the mass differences ΔM_q by means of

$$\Delta M_q = \frac{G_F^2}{6\pi^2} \eta_B m_{B_q} (\hat{B}_{B_q} F_{B_q}^2) M_W^2 S(x_t, 1/R) |V_{tq}|^2, \quad (3.11)$$

where F_{B_q} is the B_q -meson decay constant and \hat{B}_q the renormalization group invariant parameter related to the hadronic matrix element of the operator $Q(\Delta B = 2)$, see [25] for details. This

implies two useful formulae

$$\Delta M_d = 0.50/\text{ps} \cdot \left[\frac{\sqrt{\hat{B}_{B_d}} F_{B_d}}{230 \text{ MeV}} \right]^2 \left[\frac{|V_{td}|}{7.8 \cdot 10^{-3}} \right]^2 \left[\frac{\eta_B}{0.55} \right] \left[\frac{S(x_t, 1/R)}{2.34} \right] \quad (3.12)$$

and

$$\Delta M_s = 18.4/\text{ps} \cdot \left[\frac{\sqrt{\hat{B}_{B_s}} F_{B_s}}{270 \text{ MeV}} \right]^2 \left[\frac{|V_{ts}|}{0.040} \right]^2 \left[\frac{\eta_B}{0.55} \right] \left[\frac{S(x_t, 1/R)}{2.34} \right]. \quad (3.13)$$

The implications of these results for $|V_{td}|$, ΔM_s and the unitarity triangle will be discussed below.

Finally, a few comments regarding the QCD factor η_B are in order. This factor as given in (3.3) has been calculated within the SM including NLO QCD corrections that are mandatory for the proper matching of the Wilson coefficient of the operator $Q(\Delta B = 2)$ with its hadronic matrix element represented by the parameter $\hat{B}_{B_{s,d}}$ and calculated by means of non-perturbative methods. As the top quark and the KK modes are integrated out at a single scale $\mu_t = \mathcal{O}(m_t, 1/R)$, the contributions to η_B from scales lower than μ_t are the same for the SM and the ACD model. They simply describe the finite renormalization of $Q(\Delta B = 2)$ from scales $\mathcal{O}(\mu_t)$ down to the scales $\mathcal{O}(m_b)$. The difference between QCD corrections to the SM contributions and to the KK contributions arises only in the full theory at scales $\mu_t = \mathcal{O}(m_t, 1/R)$ as the unknown QCD corrections to the box diagrams in fig. 1 can in principle differ from the known QCD corrections to the SM box diagrams [23, 24] that have been included in η_B . As the QCD coupling constant $\alpha_s(\mu_t)$ is small and the QCD corrections to the SM box diagrams of order of a few percent, we do not expect that the difference between the QCD corrections to the diagrams in fig. 1 and to the SM box diagrams is relevant, in particular in view of the fact that the KK contributions amount to at most 17% of the full result.

For $\mu \gg \mu_t$, $\alpha_s(\mu)$ in the ACD model becomes larger [26] and the QCD corrections to KK modes with $n \gg 1$ could in principle be substantial. However, as seen in fig. 2 (a), these heavy modes give only a tiny contribution to $S(x_t, 1/R)$ and can be safely neglected.

3.2 ε_K

The effective Hamiltonian for $\Delta S = 2$ transitions is given in the ACD model as follows

$$\begin{aligned} \mathcal{H}_{\text{eff}}^{\Delta S=2} = & \frac{G_F^2}{16\pi^2} M_W^2 \left[\lambda_c^2 \eta_1 S_0(x_c) + \lambda_t^2 \eta_2 S(x_t, 1/R) + 2\lambda_c \lambda_t \eta_3 S_0(x_c, x_t) \right] \times \\ & \times \left[\alpha_s^{(3)}(\mu) \right]^{-2/9} \left[1 + \frac{\alpha_s^{(3)}(\mu)}{4\pi} J_3 \right] Q(\Delta S = 2) + h.c. \end{aligned} \quad (3.14)$$

where $\lambda_i = V_{is}^* V_{id}$, $\alpha_s^{(3)}$ is the strong coupling constant in an effective three flavour theory and $J_3 = 1.895$ in the NDR scheme [23]. In (3.14), the relevant operator

$$Q(\Delta S = 2) = (\bar{s}d)_{V-A}(\bar{s}d)_{V-A}, \quad (3.15)$$

is multiplied by the corresponding Wilson coefficient function. This function is decomposed into a charm-, a top- and a mixed charm-top contribution. The SM function $S_0(x_c, x_t)$ is defined by

$$S_0(x_c, x_t) = F(x_c, x_t) + F(x_u, x_u) - F(x_c, x_u) - F(x_t, x_u), \quad (3.16)$$

where $F(x_i, x_j)$ is the true function corresponding to the box diagrams with (i, j) exchanges. One has

$$S_0(x_c, x_t) = x_c \left[\ln \frac{x_t}{x_c} - \frac{3x_t}{4(1-x_t)} - \frac{3x_t^2 \ln x_t}{4(1-x_t)^2} \right], \quad (3.17)$$

where we keep only linear terms in $x_c \ll 1$, but of course all orders in x_t .

In view of the comments made after (3.8) and the structure of (3.16), the impact of the KK modes on the charm- and mixed charm-top contributions is totally negligible and we take into account these modes only in the top contribution that is described by the same function $S(x_t, 1/R)$ as in the case of ΔM_q . This also means that the $K_L - K_S$ mass difference, ΔM_K , being dominated by internal charm contributions in (3.14) is practically unaffected by the KK modes.

Short distance QCD effects are described through the correction factors η_1, η_2, η_3 and the explicitly α_s -dependent terms in (3.14). The NLO values of η_i are given as follows [27, 23, 28]:

$$\eta_1 = 1.45 \pm 0.38, \quad \eta_2 = 0.57 \pm 0.01, \quad \eta_3 = 0.47 \pm 0.04. \quad (3.18)$$

The standard procedure allows now to calculate the CP-violating parameter ε_K [25]

$$\varepsilon_K = C_\varepsilon \hat{B}_K \text{Im} \lambda_t \{ \text{Re} \lambda_c [\eta_1 S_0(x_c) - \eta_3 S_0(x_c, x_t)] - \text{Re} \lambda_t \eta_2 S(x_t, 1/R) \} \exp(i\pi/4), \quad (3.19)$$

where $C_\varepsilon = 3.837 \cdot 10^4$ is a numerical constant. \hat{B}_K is the renormalization group invariant parameter related to the hadronic matrix element of the operator $Q(\Delta S = 2)$, see [25] for details.

3.3 Unitarity Triangle in the ACD Model

What is the impact of the KK contributions to the function S on the elements of the CKM matrix and in particular on the shape of the unitarity triangle? In order to answer this question let us recall a few aspects of the unitarity triangle (UT) shown in fig. 3 and of the Wolfenstein

parametrization [29] as generalized to higher orders in λ in [30]. The apex of the unitarity triangle is given by [30]

$$\bar{\varrho} = \varrho(1 - \frac{\lambda^2}{2}), \quad \bar{\eta} = \eta(1 - \frac{\lambda^2}{2}). \quad (3.20)$$

Here λ , A , ϱ and η are the Wolfenstein parameters [29]. Moreover, one has

$$V_{us} = \lambda + \mathcal{O}(\lambda^7), \quad V_{ub} = A\lambda^3(\varrho - i\eta), \quad V_{cb} = A\lambda^2 + \mathcal{O}(\lambda^8), \quad (3.21)$$

$$V_{ts} = -A\lambda^2 + \frac{1}{2}A\lambda^4[1 - 2(\varrho + i\eta)], \quad V_{td} = A\lambda^3(1 - \bar{\varrho} - i\bar{\eta}). \quad (3.22)$$

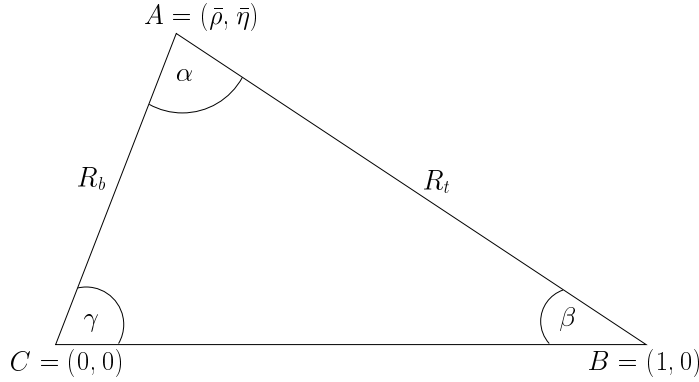


Figure 3: Unitarity Triangle.

The lengths R_b and R_t are given by

$$R_b \equiv \frac{|V_{ud}V_{ub}^*|}{|V_{cd}V_{cb}^*|} = \sqrt{\bar{\varrho}^2 + \bar{\eta}^2} = (1 - \frac{\lambda^2}{2})\frac{1}{\lambda} \left| \frac{V_{ub}}{V_{cb}} \right|, \quad (3.23)$$

$$R_t \equiv \frac{|V_{td}V_{tb}^*|}{|V_{cd}V_{cb}^*|} = \sqrt{(1 - \bar{\varrho})^2 + \bar{\eta}^2} = \frac{1}{\lambda} \left| \frac{V_{td}}{V_{cb}} \right| \quad (3.24)$$

and the angles β and γ of the UT are related directly to the complex phases of the CKM elements V_{td} and V_{ub} , respectively, through

$$V_{td} = |V_{td}|e^{-i\beta}, \quad V_{ub} = |V_{ub}|e^{-i\gamma}. \quad (3.25)$$

The five constraints on the UT that we have at our disposal at present are:

- The R_b Constraint: As seen in (3.23), the length of the side AC is determined from $|V_{ub}/V_{cb}|$.

- ε_K -Hyperbola (Indirect CP Violation in $K_L \rightarrow \pi\pi$) obtained from (3.19) and the experimental value for ε_K ($\lambda = 0.221$):

$$\bar{\eta} \left[(1 - \bar{\varrho}) A^2 \eta_2 S(x_t, 1/R) + P_c(\varepsilon) \right] A^2 \hat{B}_K = 0.214 , \quad (3.26)$$

where $P_c(\varepsilon) = 0.28 \pm 0.05$ [27, 28] represents the charm contribution that is not affected by the KK contributions.

- $B_d^0 - \bar{B}_d^0$ -Mixing Constraint (ΔM_d):

$$R_t = \frac{1}{\lambda} \frac{|V_{td}|}{|V_{cb}|} = 0.86 \cdot \left[\frac{|V_{td}|}{7.8 \cdot 10^{-3}} \right] \left[\frac{0.041}{|V_{cb}|} \right] \quad (3.27)$$

with

$$|V_{td}| = 7.8 \cdot 10^{-3} \left[\frac{230 \text{ MeV}}{\sqrt{\hat{B}_{B_d} F_{B_d}}} \right] \sqrt{\frac{\Delta M_d}{0.50/\text{ps}}} \sqrt{\frac{0.55}{\eta_B}} \sqrt{\frac{2.34}{S(x_t, 1/R)}} \quad (3.28)$$

where $\Delta M_d = (0.503 \pm 0.006)/\text{ps}$ [31].

- $B_s^0 - \bar{B}_s^0$ -Mixing Constraint ($\Delta M_d/\Delta M_s$):

$$R_t = 0.87 \sqrt{\frac{\Delta M_d}{0.50/\text{ps}}} \sqrt{\frac{18.4/\text{ps}}{\Delta M_s}} \left[\frac{\xi}{1.18} \right], \quad \xi = \frac{\sqrt{\hat{B}_s} F_{B_s}}{\sqrt{\hat{B}_d} F_{B_d}} \quad (3.29)$$

where $\Delta M_s > 14.4/\text{ps}$ at 95% C.L. [31].

- The direct measurement of $\sin 2\beta$ through the CP asymmetry $a(\psi K_S)$ in $B_d \rightarrow \psi K_S$ that is not affected by the KK contributions.

The main uncertainties in this analysis originate in the theoretical uncertainties in the non-perturbative parameters \hat{B}_K and $\sqrt{\hat{B}_d} F_{B_d}$ and to a lesser extent in ξ [32]:

$$\hat{B}_K = 0.86 \pm 0.15, \quad \sqrt{\hat{B}_d} F_{B_d} = (235_{-41}^{+33}) \text{ MeV}, \quad \xi = 1.18_{-0.04}^{+0.13}. \quad (3.30)$$

Also the uncertainties in $|V_{ub}/V_{cb}|$ and $\sqrt{\hat{B}_s} F_{B_s} = (276 \pm 38) \text{ MeV}$ are substantial. The QCD sum rules results for the parameters in question are similar and can be found in [33].

With these formulae at hand let us enumerate a few general properties of the values of the CKM elements within the ACD model. These are:

- $|V_{us}|$, $|V_{cb}|$ and $|V_{ub}|$ are usually determined from tree level decays. As in the ACD model there are no KK contributions at the tree level, the absolute values of these three CKM elements are to an excellent approximation the same as in the SM model. From the point

of view of the unitarity triangle (UT), this means that the lengths of its two sides, AC and CB are common to the SM model and the ACD model. In our numerical analysis we will use, as in [34],

$$|V_{us}| = \lambda = 0.221 \pm 0.002 \quad |V_{cb}| = (40.6 \pm 0.8) \cdot 10^{-3}, \quad (3.31)$$

$$\frac{|V_{ub}|}{|V_{cb}|} = 0.089 \pm 0.008, \quad |V_{ub}| = (3.63 \pm 0.32) \cdot 10^{-3}. \quad (3.32)$$

- The angle β of the UT has been determined recently by the BaBar [35] and Belle [36] collaborations from the CP asymmetry $a_{\psi K_S}$ in $B \rightarrow \psi K_S$ with a high accuracy giving the world grand average [37]

$$(\sin 2\beta)_{\psi K_S} = 0.734 \pm 0.054. \quad (3.33)$$

As there are no new complex phases in the ACD model beyond the KM phase, the angle β as extracted by means of $a_{\psi K_S}$ is common to both models in question.

- A similar comment applies to $|V_{td}|$ or equivalently the length R_t of the side AB in fig. 3, when R_t is extracted from the ratio $\Delta M_d/\Delta M_s$ that is independent of $S(x_t, 1/R)$ as seen in (3.29).

Thus when $|V_{ub}/V_{cb}|$, $\sin 2\beta$ from $a_{\psi K_S}$ and $\Delta M_d/\Delta M_s$ are used to construct the UT, there is no difference between the SM and the ACD model as all explicit dependence on $1/R$ cancels out. This universal UT (UUT) [14] that is valid for all MVF models, as defined in [14], has recently been determined [34, 38].

Now, even though there exists a UUT common to the SM and the ACD model, in view of the fact that $S(x_t, 1/R) \neq S_0(x_t)$, only one of these two models, if any, will have ε_K , ΔM_d and ΔM_s that agree with the experimental data. Let us consider ΔM_s first. As seen in (3.22) $|V_{ts}|$ is very close to $|V_{cb}|$ because of CKM unitarity. Therefore it is common with an excellent accuracy to both models and consequently

$$\frac{(\Delta M_s)_{\text{ACD}}}{(\Delta M_s)_{\text{SM}}} = \frac{S(x_t, 1/R)}{S_0(x_t)} > 1. \quad (3.34)$$

However, this ratio is at most 1.17 and the distinction between these two models will only be possible provided $\hat{B}_{B_s} F_{B_s}^2$ can be calculated to better than 10% accuracy. A very difficult task.

The fact that $S(x_t, 1/R) > S_0(x_t)$ implies also that with the experimentally known values of ε_K and ΔM_d , one has

$$|V_{td}|_{\text{ACD}} < |V_{td}|_{\text{SM}}, \quad \gamma_{\text{ACD}} < \gamma_{\text{SM}} \quad (3.35)$$

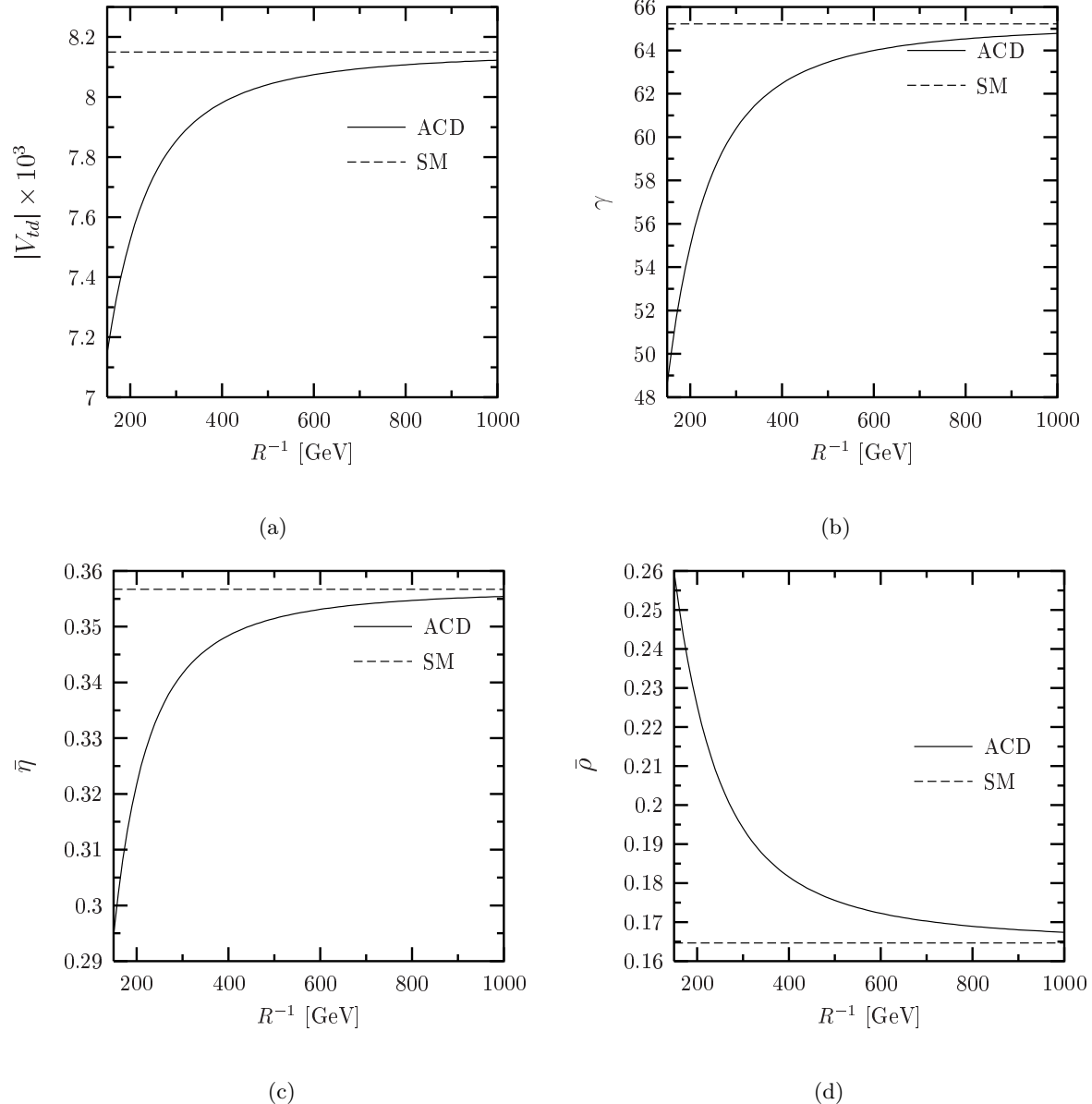


Figure 4: Results for various CKM parameters in the ACD model and in the SM: (a) $|V_{td}|$ (b) γ (c) $\bar{\eta}$ (d) $\bar{\rho}$.

as can easily be inferred from (3.26) and (3.28). In particular (3.28) implies

$$\frac{|V_{td}|_{\text{ACD}}}{|V_{td}|_{\text{SM}}} = \sqrt{\frac{S_0(x_t)}{S(x_t, 1/R)}}. \quad (3.36)$$

Thus $|V_{td}|_{\text{ACD}}$ can be smaller than $|V_{td}|_{\text{SM}}$ by at most 8%. In order to determine such a difference, more accurate information on the unitarity triangle and the non-perturbative parameters entering ε_K and $\Delta M_{d,s}$ is necessary. Similarly γ_{ACD} can be smaller than γ_{SM} by at most 10 degrees.

We illustrate these properties in fig. 4, where we show the $1/R$ dependence of $|V_{td}|$, γ , $\bar{\varrho}$ and $\bar{\eta}$. In obtaining these results we used the following procedure. First using the central value $|V_{td}|_{\text{SM}} = 0.00815$ from the SM fit of [34] and $m_t = 167$ GeV we determined $|V_{td}|_{\text{ACD}}$ by means of (3.36). The result is shown in fig. 4 (a). Using next the central values in (3.31) and (3.32) and the $1/R$ dependence of $(R_t)_{\text{ACD}} = |V_{td}|_{\text{ACD}}/(\lambda|V_{cb}|)$, we determined γ , $\bar{\varrho}$ and $\bar{\eta}$ as functions of $1/R$. We show in fig. 5 the unitarity triangles corresponding to the ACD model with $1/R = 200$ GeV and the SM model.

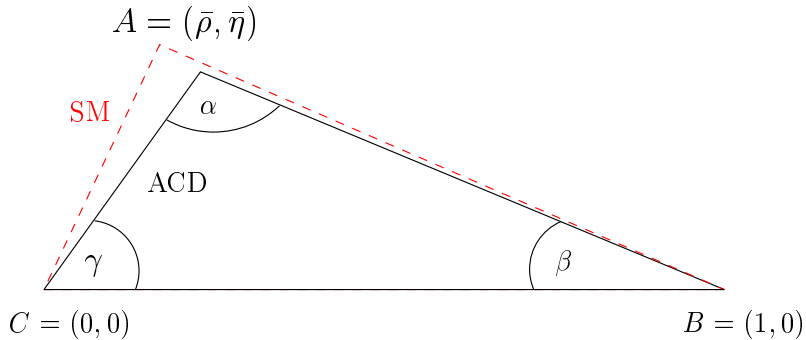


Figure 5: Unitarity Triangle in the ACD model for $1/R = 200$ GeV and in the SM.

In summary, the CKM elements in the ACD model extracted from $\Delta F = 2$ transitions and the CP asymmetry $a_{\psi K_S}$ are not expected to differ substantially from the corresponding values found within the SM. This is very fortunate as the most recent fits of the UT [34, 37, 39, 40, 41, 42] based on the SM expressions for $\Delta F = 2$ transitions agree very well with the direct measurement of the angle β by means of $a_{\psi K_S}$. With improved data on $a_{\psi K_S}$ and in particular ΔM_s and improved values for \hat{B}_K and $\hat{B}_{B_q} F_{B_q}^2$, a constraint on the compactification radius R from $\Delta F = 2$ processes is in principle possible. However, for the time being even the lowest value $1/R = 200$ GeV considered by us is consistent with the present fits of the UT. Setting $1/R = 200$ GeV and repeating the analysis of [34], that uses the bayesian method [39], one finds [43] the values for $(\bar{\varrho}, \bar{\eta})$, $\sin 2\alpha$, γ , ΔM_s and $|V_{td}|$ in the second column of table 1. For a comparison we give the corresponding ranges in the SM. To this end all input parameters of [34] have been used.

Comparing the two columns in table 1, we observe all the patterns shown in fig. 4. However, due to substantial uncertainties in the input parameters, the effects of the KK modes are partly washed out. In particular, the suppressions of $|V_{td}|$ and $\bar{\eta}$ amount to 4–5% rather than $\mathcal{O}(10\%)$ that we found in fig. 4. This is easy to understand. With no uncertainty in $\sqrt{\hat{B}_{B_d}} F_{B_d}$, the value of $|V_{td}|$ is strongly correlated with $S(x_t, 1/R)$ by means of (3.12) as ΔM_d is known very well experimentally. Once the uncertainties in $\sqrt{\hat{B}_{B_d}} F_{B_d}$ are taken into account, the enhancement of the function S in the ACD model can be compensated by the decrease of both $|V_{td}|$ and $\sqrt{\hat{B}_{B_d}} F_{B_d}$, implying a smaller suppression of $|V_{td}|$ than found in fig. 4. Similar comments can be made in connection with other quantities in table 1.

Clearly, low energy non-perturbative parameters as $\sqrt{\hat{B}_{B_d}} F_{B_d}$, \hat{B}_K and ξ do not depend on the compactification scale. On the other hand they are subject to uncertainties and it is not surprising that the fit of the unitarity triangle within the ACD model prefers lower values of $\sqrt{\hat{B}_{B_d}} F_{B_d}$ and \hat{B}_K than in the SM. The true effects of the KK modes can then only be clearly seen as in fig. 4 when the input parameters have no uncertainties. This exercise shows very clearly the importance of the reduction of the theoretical uncertainties in connection with the search for new physics.

Strategy	ACD ($1/R = 200$ GeV)	SM
$\bar{\eta}$	0.342 ± 0.027 ($0.288 - 0.398$)	0.357 ± 0.027 ($0.305 - 0.411$)
$\bar{\rho}$	0.197 ± 0.047 ($0.102 - 0.296$)	0.173 ± 0.046 ($0.076 - 0.260$)
$\sin 2\alpha$	-0.23 ± 0.25 ($-0.70 - 0.27$)	-0.09 ± 0.25 ($-0.54 - 0.40$)
γ (degrees)	59.5 ± 7.0 ($45.3 - 74.8$)	63.5 ± 7.0 ($51.0 - 79.0$)
ΔM_s (ps^{-1})	$18.6^{+1.9}_{-1.5}$ ($15.7 - 26.2$)	$18.0^{+1.7}_{-1.5}$ ($15.4 - 21.7$)
$ V_{td} $ (10^{-3})	7.80 ± 0.42 ($6.96 - 8.69$)	8.15 ± 0.41 ($7.34 - 8.97$)

Table 1: Values and errors for different quantities in the ACD model with $1/R = 200$ GeV [43] and in the SM from [34]. The 95% probability regions are given in brackets.

4 Rare K and B Decays

4.1 Preliminaries

We will now move to discuss the semileptonic rare FCNC transitions $K^+ \rightarrow \pi^+ \nu \bar{\nu}$, $K_L \rightarrow \pi^0 \nu \bar{\nu}$, $K_L \rightarrow \mu \bar{\mu}$, $B \rightarrow X_{s,d} \nu \bar{\nu}$ and $B_{s,d} \rightarrow \mu \bar{\mu}$. Within the SM and the ACD model these decays are loop-induced semileptonic FCNC processes governed by Z^0 -penguin and box diagrams and described by two functions $X(x_t, 1/R)$ and $Y(x_t, 1/R)$ for the decays with $\nu \bar{\nu}$ and $\mu \bar{\mu}$ in the final state, respectively.

A particular and very important virtue of these decays (with the exception of $K_L \rightarrow \mu \bar{\mu}$) is their clean theoretical character [25] that allows to probe high energy scales of the theory and in particular to measure V_{td} and $\text{Im} \lambda_t = \text{Im} V_{ts}^* V_{td}$ from $K^+ \rightarrow \pi^+ \nu \bar{\nu}$ and $K_L \rightarrow \pi^0 \nu \bar{\nu}$ respectively. Moreover, the combination of these two decays offers one of the cleanest measurements of $\sin 2\beta$ [44], see [44, 45] for more details.

4.2 Effective Hamiltonians for $K \rightarrow \pi \nu \bar{\nu}$ and $B \rightarrow X_s \nu \bar{\nu}$

The effective Hamiltonian for $K^+ \rightarrow \pi^+ \nu \bar{\nu}$ is given in the ACD model as follows

$$\mathcal{H}_{\text{eff}} = \frac{G_F}{\sqrt{2}} \frac{\alpha}{2\pi \sin^2 \theta_w} \sum_{l=e,\mu,\tau} \left(V_{cs}^* V_{cd} X_{\text{NL}}^l + V_{ts}^* V_{td} \eta_X X(x_t, 1/R) \right) (\bar{s}d)_{V-A} (\bar{\nu}_l \nu_l)_{V-A}. \quad (4.1)$$

The index $l=e, \mu, \tau$ denotes the lepton flavour. The dependence on the charged lepton mass resulting from the box diagram is negligible for the top contribution. In the charm sector this is the case only for the electron and the muon but not for the τ -lepton. In what follows we will set the QCD factor η_X [46, 47, 48] to unity as for $m_t \equiv \bar{m}_t(m_t)$ it equals 0.994.

The function $X(x_t, 1/R)$ relevant for the top part is given by

$$X(x_t, 1/R) = C(x_t, 1/R) + B^{\nu \bar{\nu}}(x_t, 1/R). \quad (4.2)$$

Here

$$C(x_t, 1/R) = C_0(x_t) + \sum_{n=1}^{\infty} C_n(x_t, x_n) \quad (4.3)$$

results from Z^0 -penguin diagrams with the SM contribution $C_0(x_t)$ given by

$$C_0(x_t) = \frac{x_t}{8} \left[\frac{x_t - 6}{x_t - 1} + \frac{3x_t + 2}{(x_t - 1)^2} \ln x_t \right]. \quad (4.4)$$

The sum in (4.3) represents the KK contributions that are calculated from the Feynman diagrams in fig. 6 as discussed below. Next

$$B^{\nu \bar{\nu}}(x_t, 1/R) = -4B_0(x_t) + \sum_{n=1}^{\infty} B_n^{\nu \bar{\nu}}(x_t, x_n) \quad (4.5)$$

results from box diagrams with the SM contribution given by the first term and

$$B_0(x_t) = \frac{1}{4} \left[\frac{x_t}{1-x_t} + \frac{x_t \ln x_t}{(x_t-1)^2} \right]. \quad (4.6)$$

The sum in (4.5) represents the KK contributions that are calculated from the Feynman diagrams in fig. 8 as discussed below.

The expression corresponding to $X(x_t, 1/R)$ in the charm sector is the function X_{NL}^l . It results from the NLO calculation [49] and is given explicitly in [48] where further details can be found. As in the case of the charm contributions in the $\Delta S = 2$ Hamiltonian, here the KK contributions are also negligible. The numerical values for X_{NL}^l for $\mu = m_c$ and several values of $\Lambda_{\overline{\text{MS}}}^{(4)}$ and $m_c(m_c)$ can be found in [48]. For our purposes we need only ($\lambda = 0.221$)

$$P_0(X) = \frac{1}{\lambda^4} \left[\frac{2}{3} X_{\text{NL}}^e + \frac{1}{3} X_{\text{NL}}^\tau \right] = 0.41 \pm 0.06, \quad (4.7)$$

where the error results from the variation of $\Lambda_{\overline{\text{MS}}}^{(4)}$ and $m_c(m_c)$.

In the case of $K_L \rightarrow \pi^0 \nu \bar{\nu}$ that is governed by CP-violating contributions only the top contribution in (4.1) matters. Similarly the effective Hamiltonians for $B \rightarrow X_{s,d} \nu \bar{\nu}$ is obtained from (4.1) by neglecting the charm contribution and changing appropriately the CKM factor and quark flavours. In all these decays the KK modes contribute universally only through the function $X(x_t, 1/R)$.

4.3 Effective Hamiltonians for $B_{s,d} \rightarrow \mu \bar{\mu}$ and $K_L \rightarrow \mu \bar{\mu}$

The effective Hamiltonian for $B_s \rightarrow l^+ l^-$ in the ACD model is given as follows:

$$\mathcal{H}_{\text{eff}} = -\frac{G_F}{\sqrt{2}} \frac{\alpha}{2\pi \sin^2 \theta_w} V_{tb}^* V_{ts} \eta_Y Y(x_t, 1/R) (\bar{b}s)_{V-A} (\bar{l}l)_{V-A} + h.c. \quad (4.8)$$

with s replaced by d in the case of $B_d \rightarrow l^+ l^-$. The charm contributions are fully negligible here. In what follows we will set the QCD factor η_Y [46, 47, 48] to unity as for $m_t \equiv \overline{m}_t(m_t)$ it equals 1.012.

The function $Y(x_t, 1/R)$ is given in the ACD model by

$$Y(x_t, 1/R) = C(x_t, 1/R) + B^{\mu \bar{\mu}}(x_t, 1/R), \quad (4.9)$$

with $C(x_t, 1/R)$ given in (4.3) and

$$B^{\mu \bar{\mu}}(x_t, 1/R) = -B_0(x_t) + \sum_{n=1}^{\infty} B_n^{\mu \bar{\mu}}(x_t, x_n) \quad (4.10)$$

with the first term representing the SM contribution. The second term results from the box diagrams in fig. 8.

The effective Hamiltonian for the short distance contribution to $K_L \rightarrow \mu\bar{\mu}$ is given by (4.8) with the appropriate change of the CKM factors and quark flavours and a small SM charm contribution Y_{NL} [48] in analogy to X_{NL}^l in (4.1). The relevant branching ratio will be given below.

4.4 Z^0 -Penguin Diagrams

The function $C_n(x_t, x_n)$ can be found by calculating the vertex diagrams in fig. 6 and adding an electroweak counter term as discussed in detail in [50]. The latter is found by calculating the self-energy diagrams of fig. 11 that describe flavour non-diagonal propagation of quark fields and subsequently rotating the quark fields appropriately so that this flavour non-diagonal propagation does not take place in the new fields.

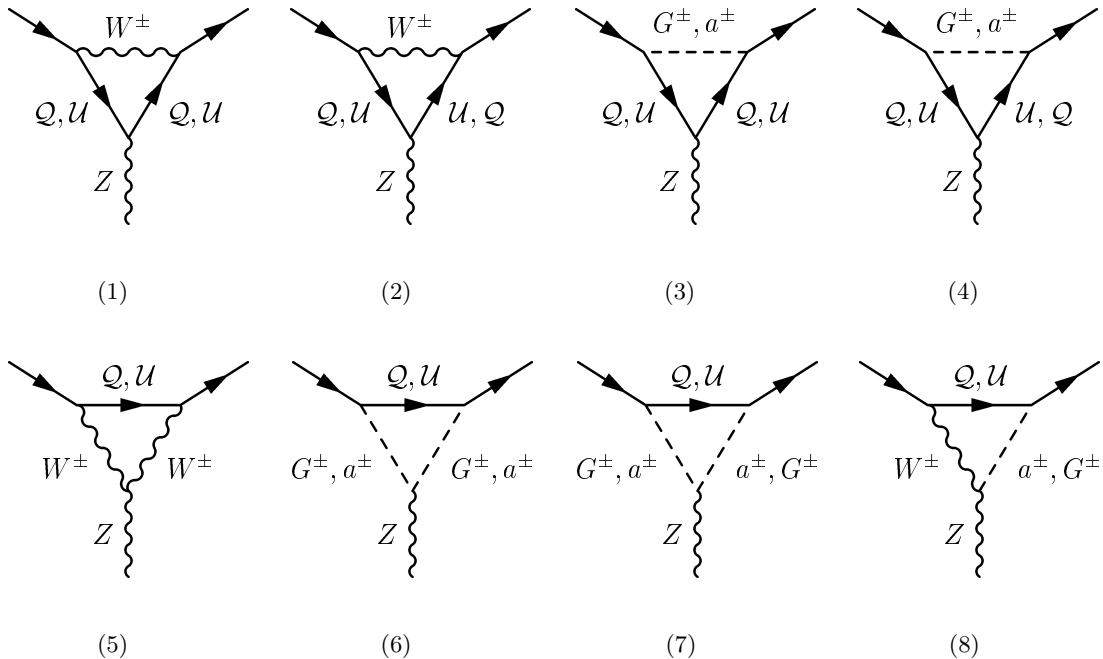


Figure 6: Penguin diagrams contributing to $C_n(x_t, x_n)$. The analytical expressions are listed in appendix C. (8) includes the additional diagram with W^\pm and (a^\pm, G^\pm) interchanged.

In the 't Hooft-Feynman gauge for the $W_{(n)}^\pm$ and $G_{(n)}^\pm$ propagators, the contribution of the diagrams in fig. 6 to the flavour-changing vertex Γ_Z^μ including the electroweak counterterm is given by

$$\Delta\Gamma_Z^\mu = i \frac{g_2^3}{16\pi^2 \cos\theta_w} V_{ts}^* V_{td} C_n(x_t, x_n) \bar{s} \gamma_\mu (1 - \gamma_5) d. \quad (4.11)$$

We neglect the external momenta in fig. 6 and the masses of external quarks. The function

$C_n(x_t, x_n)$ is defined through

$$C_n(x_t, x_n) = F(x_{t(n)}) - F(x_{u(n)}) \quad (4.12)$$

with the functions $F(x_{t(n)})$ and $F(x_{u(n)})$ representing the contributions of the $\mathcal{Q}_{t(n)}$, $\mathcal{U}_{t(n)}$ and $\mathcal{Q}_{u(n)}$, $\mathcal{U}_{u(n)}$ modes, respectively,

$$F(x_{t(n)}) = \sum_{i=1}^8 F_i(x_{t(n)}) + \left(\frac{1}{2} - \frac{1}{3} s_w^2 \right) \sum_{i=1}^2 \Delta S_i(x_{t(n)}). \quad (4.13)$$

Here $s_w \equiv \sin \theta_w$, F_i stand for the contributions of diagrams in fig. 6 and ΔS_i denote the electroweak counter terms.

The explicit contributions of various sets of diagrams to these functions are given in appendix C. Adding up these contributions we find

$$C_n(x_t, x_n) = \frac{x_t}{8(x_t - 1)^2} \left[x_t^2 - 8x_t + 7 + (3 + 3x_t + 7x_n - x_t x_n) \ln \frac{x_t + x_n}{1 + x_n} \right]. \quad (4.14)$$

In fig. 7 (a), we show $C_n(x_t, x_n)$ as a function of n/R . In this case the convergence of the sum of the KK modes is significantly improved by the GIM mechanism so that only a few first terms in the sum in (4.3) are relevant. We will return to this at the end of this section. We observe that in contrast to the function S of section 3 the diagrams involving only $W_{(n)}^\pm$ play the dominant role among the KK contributions.

In fig. 7 (b) we plot $C(x_t, 1/R)$ versus $1/R$. For $1/R = 200$ GeV we observe a 38% enhancement of the function C with respect to its SM value given by $C_0(x_t)$. For $1/R = 250$ GeV this enhancement decreases to 26% and it is 11% for $1/R = 400$ GeV. The significant enhancement of C is the origin of the enhancements of the branching ratios discussed below.

4.5 Box Diagram Contributions

The functions $B_n^{\nu\bar{\nu}}(x_t, x_n)$ and $B_n^{\mu\bar{\mu}}(x_t, x_n)$ can be found by appropriate rescaling of the box diagrams contributing to $\Delta F = 2$ transitions that we considered in section 3. It turns out that the box contributions of the KK modes are tiny. For instance for $1/R = 200$ GeV and $m_t = 167$ GeV we find $B_1^{\nu\bar{\nu}}(x_t, x_1) = 0.0098$ and $B_1^{\mu\bar{\mu}}(x_t, x_1) = 0.0049$ with even smaller values for $n > 1$ and larger $1/R$. Consequently, these contributions can be safely neglected in comparison with C_n . For completeness we give in appendix D the analytic formulae for $B_n^{\nu\bar{\nu}}(x_t, x_n)$ and $B_n^{\mu\bar{\mu}}(x_t, x_n)$.

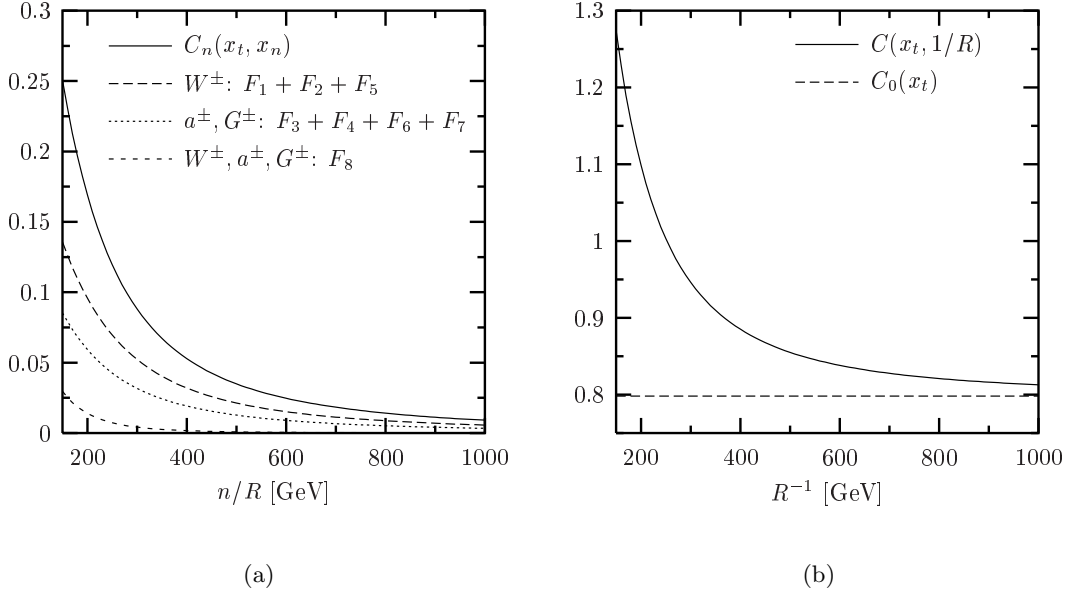


Figure 7: (a) Contribution C_n of the n^{th} KK mode to $C(x_t, 1/R)$. The functions F_i correspond to the diagrams given in fig. 6. (b) The functions $C(x_t, 1/R)$ and $C_0(x_t)$.

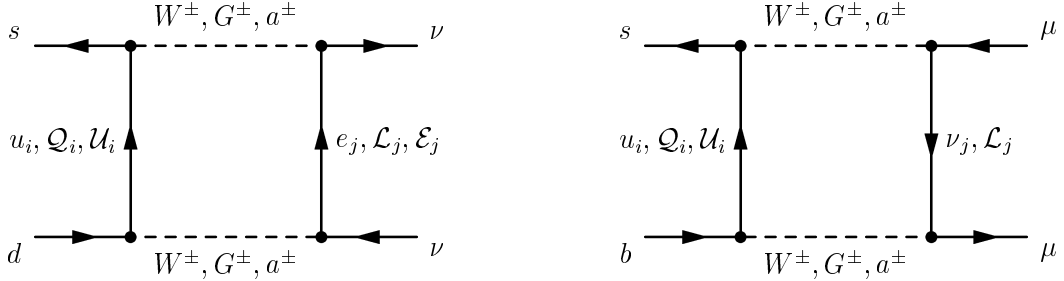


Figure 8: Box diagrams contributing to $B_n^{\nu\bar{\nu}}$ and to $B_n^{\mu\bar{\mu}}$.

4.6 The Functions \mathbf{X} and \mathbf{Y}

Neglecting the box contributions of the KK modes we find

$$X(x_t, 1/R) = X_0(x_t) + \sum_{n=1}^{\infty} C_n(x_t, x_n) \equiv X_0(x_t) + \Delta X , \quad (4.15)$$

$$Y(x_t, 1/R) = Y_0(x_t) + \sum_{n=1}^{\infty} C_n(x_t, x_n) \equiv Y_0(x_t) + \Delta Y \quad (4.16)$$

with ($m_t = 167$ GeV)

$$X_0(x_t) = \frac{x_t}{8} \left[\frac{x_t + 2}{x_t - 1} + \frac{3x_t - 6}{(x_t - 1)^2} \ln x_t \right] = 1.526 , \quad (4.17)$$

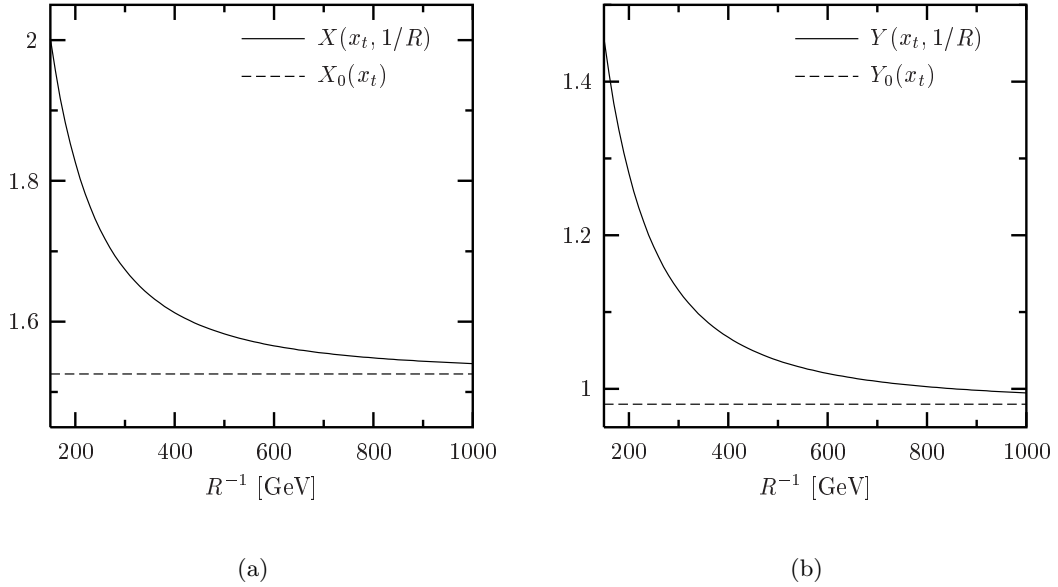


Figure 9: The functions (a) $X(x_t, 1/R)$ and $X_0(x_t)$ and (b) $Y(x_t, 1/R)$ and $Y_0(x_t)$.

$$Y_0(x_t) = \frac{x_t}{8} \left[\frac{x_t - 4}{x_t - 1} + \frac{3x_t}{(x_t - 1)^2} \ln x_t \right] = 0.980 \quad (4.18)$$

summarizing the SM contributions and $\Delta X = \Delta Y$ representing the corrections due to KK modes.

In fig. 9 we plot $X(x_t, 1/R)$ and $Y(x_t, 1/R)$ versus $1/R$. We observe that due to the inequality $X_0 > Y_0$ the relative impact of the KK modes is larger in the function Y . For $1/R = 200$ GeV the functions X and Y are enhanced by 20% and 31%, respectively. For $1/R = 250$ GeV this enhancement decrease to 13%(21%) and are only 6%(9%) for $1/R = 400$ GeV.

In table 2 we give the values of the functions S , C , X and Y for different $1/R$ and $m_t = 167$ GeV.

$1/R$ [GeV]	S	C	X	Y
200	2.813	1.099	1.826	1.281
250	2.664	1.003	1.731	1.185
300	2.582	0.946	1.674	1.128
400	2.500	0.885	1.613	1.067
SM	2.398	0.798	1.526	0.980

Table 2: Values for the functions S , C , X and Y .

4.7 Branching Ratios for Rare Decays

The branching ratios for the rare decays in question can be directly obtained from [25] by simply replacing the SM functions X_0 and Y_0 by $X(x_t, 1/R)$ and $Y(x_t, 1/R)$, respectively. We have

$$Br(K^+ \rightarrow \pi^+ \nu \bar{\nu}) = \kappa_+ \cdot \left[\left(\frac{\text{Im} \lambda_t}{\lambda^5} X(x_t, 1/R) \right)^2 + \left(\frac{\text{Re} \lambda_c}{\lambda} P_0(X) + \frac{\text{Re} \lambda_t}{\lambda^5} X(x_t, 1/R) \right)^2 \right], \quad (4.19)$$

$$\kappa_+ = r_{K^+} \frac{3\alpha^2 Br(K^+ \rightarrow \pi^0 e^+ \nu)}{2\pi^2 \sin^4 \theta_w} \lambda^8 = 4.31 \cdot 10^{-11}, \quad (4.20)$$

where we have used [51]

$$\alpha = \frac{1}{129}, \quad \sin^2 \theta_w = 0.23, \quad Br(K^+ \rightarrow \pi^0 e^+ \nu) = 4.87 \cdot 10^{-2}. \quad (4.21)$$

Here $\lambda_i = V_{is}^* V_{id}$ with λ_c being real to a very high accuracy. $r_{K^+} = 0.901$ summarizes isospin breaking corrections [52] in relating $K^+ \rightarrow \pi^+ \nu \bar{\nu}$ to $K^+ \rightarrow \pi^0 e^+ \nu$. $P_0(X)$ is given in (4.7).

Next,

$$Br(K_L \rightarrow \pi^0 \nu \bar{\nu}) = \kappa_L \cdot \left(\frac{\text{Im} \lambda_t}{\lambda^5} X(x_t, 1/R) \right)^2, \quad (4.22)$$

$$\kappa_L = \frac{r_{K_L}}{r_{K^+}} \frac{\tau(K_L)}{\tau(K^+)} \kappa_+ = 1.88 \cdot 10^{-10} \quad (4.23)$$

with κ_+ given in (4.20) and $r_{K_L} = 0.944$ summarizing isospin breaking corrections in relating $K_L \rightarrow \pi^0 \nu \bar{\nu}$ to $K^+ \rightarrow \pi^0 e^+ \nu$ [52].

Next, normalizing to $Br(B \rightarrow X_c e \bar{\nu})$ and summing over three neutrino flavours we find

$$\frac{Br(B \rightarrow X_s \nu \bar{\nu})}{Br(B \rightarrow X_c e \bar{\nu})} = \frac{3\alpha^2}{4\pi^2 \sin^4 \theta_w} \frac{|V_{ts}|^2}{|V_{cb}|^2} \frac{X^2(x_t, 1/R)}{f(z)} \frac{\kappa(0)}{\kappa(z)}. \quad (4.24)$$

Here $f(z)$ is the phase-space factor for $B \rightarrow X_c e \bar{\nu}$ with $z = m_c^2/m_b^2$ and $\kappa(z) = 0.88$ [53, 54] is the corresponding QCD correction. The factor $\kappa(0) = 0.83$ represents the QCD correction to the matrix element of the $b \rightarrow s \nu \bar{\nu}$ transition due to virtual and bremsstrahlung contributions. In the case of $B \rightarrow X_d \nu \bar{\nu}$ one has to replace V_{ts} by V_{td} which results in a decrease of the branching ratio by roughly an order of magnitude. In our numerical calculations we set $f(z) = 0.54$ and $Br(B \rightarrow X_c e \bar{\nu}) = 0.104$.

Next, the branching ratio for $B_s \rightarrow l^+ l^-$ is given by

$$Br(B_s \rightarrow l^+ l^-) = \tau(B_s) \frac{G_F^2}{\pi} \left(\frac{\alpha}{4\pi \sin^2 \theta_w} \right)^2 F_{B_s}^2 m_l^2 m_{B_s} \sqrt{1 - 4 \frac{m_l^2}{m_{B_s}^2}} |V_{tb}^* V_{ts}|^2 Y^2(x_t, 1/R) \quad (4.25)$$

where F_{B_s} is the B_s meson decay constant. The formula for $Br(B_d \rightarrow l^+l^-)$ is obtained by replacing s by d . The relevant input parameters are [32]

$$F_{B_d} = (203^{+27}_{-34}) \text{ MeV}, \quad F_{B_s} = (238 \pm 31) \text{ MeV}. \quad (4.26)$$

We set also $\tau(B_s) = 1.46$ ps and $\tau(B_d) = 1.54$ ps [51]. The short distance contribution to the dispersive part of $K_L \rightarrow \mu^+\mu^-$ is given by [46, 49]

$$Br(K_L \rightarrow \mu^+\mu^-)_{\text{SD}} = \kappa_\mu \left[\frac{\text{Re}\lambda_c}{\lambda} P_0(Y) + \frac{\text{Re}\lambda_t}{\lambda^5} Y(x_t, 1/R) \right]^2, \quad (4.27)$$

$$\kappa_\mu = \frac{\alpha^2 Br(K^+ \rightarrow \mu^+\nu)}{\pi^2 \sin^4 \theta_w} \frac{\tau(K_L)}{\tau(K^+)} \lambda^8 = 1.733 \cdot 10^{-9}, \quad (4.28)$$

where we have used $Br(K^+ \rightarrow \mu^+\nu) = 0.634$. The charm contribution including NLO corrections is given by [48]

$$P_0(Y) = \frac{Y_{\text{NL}}}{\lambda^4} = 0.128 \pm 0.013. \quad (4.29)$$

Unfortunately due to long distance contributions to the dispersive part of $K_L \rightarrow \mu^+\mu^-$, the extraction of $Br(K_L \rightarrow \mu^+\mu^-)_{\text{SD}}$ from the data is subject to considerable uncertainties. The present best estimate reads [55]

$$Br(K_L \rightarrow \mu^+\mu^-)_{\text{SD}} \leq 2.5 \cdot 10^{-9}. \quad (4.30)$$

4.8 GIM Mechanism and Convergence of the KK Sum

The tree-level masses of the KK modes of all particles approach the value n/R for large KK mode numbers n , see eq. (2.30) and (A.2). Due to the unitary CKM matrix the GIM mechanism [12] comes into play. It suppresses partly the higher KK mode contributions to the sums in eq. (3.4), (4.2), (4.5) and (4.10) and is essential for the determination of the dominant contributions. For the S_n function the GIM suppression amounts to an additional factor of $1/n^4$ for the contributions WW , GG and WG . The contributions from diagrams with a^\pm are not suppressed due to the second term in the coupling $m_4^{(t)}$, see (A.3). This results in a hierarchy of the various contributions to S_n with WW , GG and WG proportional to $1/n^6$, Wa and Ga proportional to $1/n^4$ and the dominant contribution aa proportional to $1/n^2$ for large values of n .

For the penguin diagrams the effect of the GIM mechanism on the convergence of the particular contributions is partly hidden by the subtle cancellation of divergencies among the different

contributions and the two self-energy diagrams. For the combinations plotted in fig. 7 we observe that the term corresponding to $W^\pm : F_1 + F_2 + F_5$ is logarithmically divergent without GIM and shows a $1/n^2$ behaviour after GIM mechanism has been taken into account. The $a^\pm, G^\pm : F_3 + F_4 + F_6 + F_7$ term shows no GIM suppression and is proportional to $1/n^2$ for large values of n . The mixed term $W^\pm, a^\pm, G^\pm : F_8$ is constant for large n before the inclusion of GIM mechanism, but is GIM suppressed by a factor of $1/n^2$.

The contributions to $B_n^{\nu\bar{\nu}}$ and $B_n^{u\bar{u}}$ show a $1/n^4$ behaviour with and without GIM, except the G_{WW} and H_{WW} terms. They are proportional to $1/n^2$ without GIM and behave like $1/n^4$ with GIM suppression at work. The difference to the S_n function of the asymptotic behaviour is due to the appearance of leptons with negligible zero-mode masses instead of quarks in the box diagrams contribution to the functions G and H , see eq. (A.3).

4.9 Numerical Analysis

As discussed in section 3, $|V_{td}|$, $\bar{\varrho}$ and $\bar{\eta}$ in the SM and in the ACD model differ from each other. In our numerical analysis we will take this difference into account. Not taking this difference into account would misrepresent significantly the patterns of the enhancements of branching ratios in question.

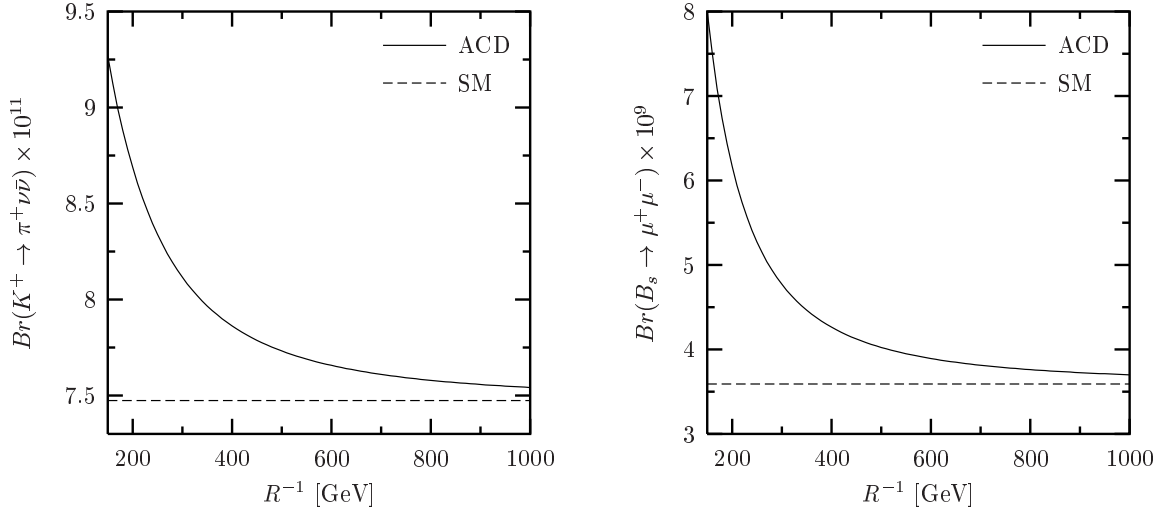


Figure 10: Branching ratio for the decays $K^+ \rightarrow \pi^+ \nu\bar{\nu}$ and $B_s \rightarrow \mu^+ \mu^-$ as predicted by the ACD model and the SM as functions of the inverse radius R of the extra dimension.

In fig. 10 we show the branching ratios $Br(K^+ \rightarrow \pi^+ \nu\bar{\nu})$ and $Br(B_s \rightarrow \mu^+ \mu^-)$ as functions of the compactification scale $1/R$. As $|V_{ts}|_{ACD} = |V_{ts}|_{SM}$, the enhancement of $Br(B_s \rightarrow \mu^+ \mu^-)$ is entirely governed by the ratio $(Y/Y_0)^2$. On the other hand the dependence of $Br(K^+ \rightarrow \pi^+ \nu\bar{\nu})$ on $1/R$ differs from the one of $(X/X_0)^2$ because of the additional charm contribution that is

independent of $1/R$ and the fact that V_{td} in the ACD model differs from its SM value. The remaining branching ratios are shown in table 3. The $1/R$ dependence of $Br(B \rightarrow X_s \nu \bar{\nu})$ is governed by the function $X^2(x_t/1/R)$, while the corresponding dependences of $Br(B \rightarrow X_d \nu \bar{\nu})$, $Br(K_L \rightarrow \pi^0 \nu \bar{\nu})$, $Br(B_d \rightarrow \mu^+ \mu^-)$ and $Br(K_L \rightarrow \mu^+ \mu^-)_{\text{SD}}$ include also the $1/R$ dependence of V_{td} shown in fig. 4 (a). As expected, all the branching ratios are significantly enhanced for $1/R \leq 300 \text{ GeV}$. For $1/R \geq 400 \text{ GeV}$, except for $Br(B_s \rightarrow \mu^+ \mu^-)$, the distinction between the predictions of the ACD model and the SM will be essentially impossible.

$1/R$	200 GeV	250 GeV	300 GeV	400 GeV	SM
$Br(K^+ \rightarrow \pi^+ \nu \bar{\nu}) \times 10^{11}$	8.70	8.36	8.13	7.88	7.49
$Br(K_L \rightarrow \pi^0 \nu \bar{\nu}) \times 10^{11}$	3.26	3.17	3.09	2.98	2.80
$Br(K_L \rightarrow \mu^+ \mu^-)_{\text{SD}} \times 10^9$	1.10	1.00	0.95	0.88	0.79
$Br(B \rightarrow X_s \nu \bar{\nu}) \times 10^5$	5.09	4.56	4.26	3.95	3.53
$Br(B \rightarrow X_d \nu \bar{\nu}) \times 10^6$	1.80	1.70	1.64	1.58	1.47
$Br(B_s \rightarrow \mu^+ \mu^-) \times 10^9$	6.18	5.28	4.78	4.27	3.59
$Br(B_d \rightarrow \mu^+ \mu^-) \times 10^{10}$	1.56	1.41	1.32	1.22	1.07

Table 3: Branching ratios for rare decays in the ACD model and the SM as discussed in the text.

In this numerical analysis we have used the results for the CKM parameters of fig. 4 and the central values of all the remaining input parameters as given above. The uncertainties in these parameters partly cover the differences between the ACD model and the SM model and it is essential to reduce these uncertainties considerably if one wants to see the effects of the KK modes in the branching ratios in question. Therefore a detailed analysis that includes all uncertainties would be in our opinion premature at present.

4.10 An Upper Bound on $Br(K^+ \rightarrow \pi^+ \nu \bar{\nu})$ in the ACD Model

The enhancement of $Br(K^+ \rightarrow \pi^+ \nu \bar{\nu})$ in the ACD model is interesting in view of the results from the AGS E787 collaboration at Brookhaven [56] that read

$$Br(K^+ \rightarrow \pi^+ \nu \bar{\nu}) = (15.7_{-8.2}^{+17.5}) \cdot 10^{-11} \quad (4.31)$$

with the central value by a factor of 2 above the SM expectation. Even if the errors are substantial and this result is compatible with the SM, the ACD model with a low compactification scale is closer to the data. As emphasized in [56, 57] the central value in (4.31) implies within the SM a value for $|V_{td}|$ that is substantially higher than the value obtained from the standard

analysis of the UT of section 3. Here we would like to emphasize that within the ACD model $Br(K^+ \rightarrow \pi^+ \nu \bar{\nu})$ is closer to the data in spite of the fact that $|V_{td}|_{\text{ACD}} < |V_{td}|_{\text{SM}}$. The enhanced Z^0 -vertex represented by the function C is responsible for this behaviour.

In [48] an upper bound on $Br(K^+ \rightarrow \pi^+ \nu \bar{\nu})$ has been derived within the SM. This bound depends only on $|V_{cb}|$, X_0 , ξ and $\Delta M_d/\Delta M_s$. With the precise value for the angle β now available this bound can be turned into a useful formula for $Br(K^+ \rightarrow \pi^+ \nu \bar{\nu})$ [57] that expresses this branching ratio in terms of theoretically clean observables. In the ACD model this formula reads:

$$Br(K^+ \rightarrow \pi^+ \nu \bar{\nu}) = \bar{\kappa}_+ |V_{cb}|^4 X^2(x_t, 1/R) \left[\sigma R_t^2 \sin^2 \beta + \frac{1}{\sigma} \left(R_t \cos \beta + \frac{\lambda^4 P_0(X)}{|V_{cb}|^2 X(x_t, 1/R)} \right)^2 \right], \quad (4.32)$$

where $\sigma = 1/(1 - \lambda^2/2)^2$, $\bar{\kappa}_+ = \kappa_+/\lambda^8$ and R_t is given in (3.29). This formula is theoretically very clean and does not involve hadronic uncertainties except for ξ in (3.29) and to a lesser extent in $|V_{cb}|$.

In order to find the upper bound on $Br(K^+ \rightarrow \pi^+ \nu \bar{\nu})$ in the ACD model we use

$$|V_{cb}| \leq 0.0422, \quad P_0(X) < 0.47, \quad \sin \beta = 0.40, \quad m_t < 172 \text{ GeV}, \quad (4.33)$$

where we have set $\sin \beta$ to its central value (see (3.33)) as $Br(K^+ \rightarrow \pi^+ \nu \bar{\nu})$ depends very weakly on it. The bound on $|V_{cb}|$ results from $|V_{cb}| = 0.0406 \pm 0.0008$ [34]. We used here two standard deviations as the determination of $|V_{cb}|$ involves some hadronic uncertainties. The result of this exercise is shown in table 4. We give there $Br(K^+ \rightarrow \pi^+ \nu \bar{\nu})_{\text{max}}$ as a function of ξ and $1/R$ for two different values of ΔM_s . The range for ξ chosen by us is in accordance with (3.30) and the recent new analysis in [58] that gives $\xi = 1.22 \pm 0.07$. The upper bound in the SM given in the last column is lower than the values for $1/R = 400$ GeV by roughly 10%. We observe that for $1/R = 200$ GeV and $\xi = 1.30$ the maximal value for $Br(K^+ \rightarrow \pi^+ \nu \bar{\nu})$ in the ACD model is rather close to the central value in (4.31).

At first sight the 30% enhancement of $Br(K^+ \rightarrow \pi^+ \nu \bar{\nu})$ for $1/R = 200$ GeV with respect to the SM values seems to contradict the results in table 3, where a more modest enhancement of $Br(K^+ \rightarrow \pi^+ \nu \bar{\nu})$ is seen. However, one should realize that now $\Delta M_d/\Delta M_s$ and not ΔM_d alone enters the analysis and the enhancement of the function X is not accompanied by a suppression of $|V_{td}|$, that with R_t given by (3.29), equals the one in the SM. The consistency with the experimental value of ΔM_d requires then a sufficiently small $\sqrt{\hat{B}_{B_d}} F_{B_d}$. In table 4 we indicate by a star the cases that require $\sqrt{\hat{B}_{B_d}} F_{B_d} \leq 190$ MeV. Such low values are rather improbable in view of (3.30) and consequently values of $Br(K^+ \rightarrow \pi^+ \nu \bar{\nu})$ larger than $12 \cdot 10^{-11}$ are rather unlikely even in the ACD model.

ξ	$1/R = 200$ GeV	$1/R = 250$ GeV	$1/R = 300$ GeV	$1/R = 400$ GeV	SM
1.30	13.8* (12.3*)	12.7* (11.3*)	12.0* (10.7)	11.3* (10.1)	10.8 (9.3)
1.25	13.0* (11.6)	12.0 (10.7)	11.4 (10.2)	10.7 (9.6)	10.3 (8.8)
1.20	12.2* (10.9)	11.3 (10.1)	10.7 (9.6)	10.1 (9.1)	9.7 (8.4)
1.15	11.5 (10.3)	10.6 (9.5)	10.1 (9.0)	9.5 (8.5)	9.1 (7.9)

Table 4: Upper bound on $Br(K^+ \rightarrow \pi^+ \nu \bar{\nu})$ in units of 10^{-11} for different values of ξ and $1/R$ and $\Delta M_s = 18/\text{ps}$ (21/ ps). The stars indicate the results corresponding to $\sqrt{\hat{B}_{B_d} F_{B_d}} \leq 190 \text{ MeV}$.

5 Summary and Outlook

In this paper we have calculated for the first time the contributions of the Kaluza-Klein (KK) modes to ΔM_K , ε_K , $\Delta M_{d,s}$ and rare decays $K^+ \rightarrow \pi^+ \nu \bar{\nu}$, $K_L \rightarrow \pi^0 \nu \bar{\nu}$, $K_L \rightarrow \mu^+ \mu^-$, $B \rightarrow X_{s,d} \nu \bar{\nu}$ and $B_{s,d} \rightarrow \mu \bar{\mu}$ in the Appelquist, Cheng and Dobrescu (ACD) model with one universal extra dimension. As a byproduct we have given a list of the required Feynman rules that have not been presented in the literature so far.

The nice property of this extension of the SM is the presence of only a single new parameter, $1/R$. This economy in new parameters should be contrasted with supersymmetric theories and models with an extended Higgs sector. Taking $1/R = 200$ GeV our findings are as follows:

- The short distance one-loop function $S(x_t, 1/R)$ relevant for $\Delta F = 2$ transitions is larger than the corresponding SM function $S_0(x_t)$ by roughly 17%. This implies on the basis of ε_K and ΔM_d a 8% suppression of $|V_{td}|_{\text{ACD}}$ with respect to $|V_{td}|_{\text{SM}}$ and a decrease of the angle γ_{ACD} by 10° with respect to γ_{SM} . On the other hand, $(\Delta M_s)_{\text{ACD}}$ is larger than $(\Delta M_s)_{\text{SM}}$ by 17%, see section 3 for details. ΔM_K is essentially unaffected.
- In order to see whether the modifications of the SM expectations are required by the data, the comparison of $|V_{td}|$ and γ extracted from ε_K and ΔM_d in the SM and in the ACD model with the universal unitarity triangle constructed by means of $|V_{ub}/V_{cb}|$, $\Delta M_d/\Delta M_s$ and $a(\psi K_S)$ will be important. To this end, the data on these quantities have to be improved and the uncertainties in the relevant non-perturbative parameters reduced.
- The short distance one-loop function $X(x_t, 1/R)$ relevant for the decays $K^+ \rightarrow \pi^+ \nu \bar{\nu}$, $K_L \rightarrow \pi^0 \nu \bar{\nu}$ and $B \rightarrow X_{s,d} \nu \bar{\nu}$ is larger than the corresponding SM function $X_0(x_t)$ by roughly 20% due to KK contributions to the Z^0 -penguins. In the case of $K^+ \rightarrow \pi^+ \nu \bar{\nu}$, $K_L \rightarrow \pi^0 \nu \bar{\nu}$ and $B \rightarrow X_{d} \nu \bar{\nu}$ this enhancement is partially compensated by the fact that $|V_{td}|_{\text{ACD}} < |V_{td}|_{\text{SM}}$ and $\bar{\eta}_{\text{ACD}} < \bar{\eta}_{\text{SM}}$. We then find the enhancements of $Br(K^+ \rightarrow \pi^+ \nu \bar{\nu})$,

$Br(K_L \rightarrow \pi^0 \nu \bar{\nu})$ and $Br(B \rightarrow X_d \nu \bar{\nu})$ over the SM expectations by 16%, 17% and 22%, respectively. As $B \rightarrow X_s \nu \bar{\nu}$ is governed by the CKM element $|V_{ts}|$ that is common to the SM and the ACD model, the enhancement of $Br(B \rightarrow X_s \nu \bar{\nu})$ amounts to 44%.

- The short distance one-loop function $Y(x_t, 1/R)$ relevant for the decays $B_{d,s} \rightarrow \mu \bar{\mu}$ and $K_L \rightarrow \mu \bar{\mu}$, is larger than the corresponding SM function $Y_0(x_t)$ by roughly 30%. As $B_s \rightarrow \mu \bar{\mu}$ is governed by the CKM element $|V_{ts}|$ this implies a 72% enhancement of $Br(B_s \rightarrow \mu \bar{\mu})$ relative to the SM expectation. In the case of $B_d \rightarrow \mu \bar{\mu}$ and $K_L \rightarrow \mu \bar{\mu}$, due to $|V_{td}|_{\text{ACD}} < |V_{td}|_{\text{SM}}$, the corresponding enhancements amount to 38% and 46%.
- As the ACD model belongs to the class of MFV models, general properties of these models identified in [14, 59] are automatically valid here.
- For $1/R = 250$ (300) GeV all these effects are decreased roughly by a factor of 1.5 (2.0). See fig. 10 and table 3.

In short, the signatures of the deviations from the SM expectations are:

- The decrease of $|V_{td}|$, γ , $\bar{\eta}$ and $\bar{\varrho}$.
- The increase of ΔM_s .
- The increase of all branching ratios considered in this paper with a hierarchical structure of maximal enhancements: $K^+ \rightarrow \pi^+ \nu \bar{\nu}$ (16%), $K_L \rightarrow \pi^0 \nu \bar{\nu}$ (17%), $B \rightarrow X_d \nu \bar{\nu}$ (22%), $K_L \rightarrow \mu \bar{\mu}$ (38%), $B \rightarrow X_s \nu \bar{\nu}$ (44%), $B_d \rightarrow \mu \bar{\mu}$ (46%) and $B_s \rightarrow \mu \bar{\mu}$ (72%) for $1/R = 200$ GeV. For $1/R = 250$ (300) GeV these enhancements are decreased roughly by a factor of 1.5 (2.0).

In the coming years of particular interest will be the improved measurements of $Br(K^+ \rightarrow \pi^+ \nu \bar{\nu})$ and ΔM_s . Indeed, in the MFV models $Br(K^+ \rightarrow \pi^+ \nu \bar{\nu})$ can be predicted as a function of X once the angle β and $\Delta M_d/\Delta M_s$ are known. The relevant formula is given in (4.32). For a given value of X , the branching ratio $Br(K^+ \rightarrow \pi^+ \nu \bar{\nu})$ decreases with increasing ΔM_s . If the present central experimental values for $Br(K^+ \rightarrow \pi^+ \nu \bar{\nu})$ will remain while the experimental error will decrease significantly, the SM expectations for $Br(K^+ \rightarrow \pi^+ \nu \bar{\nu})$ will be significantly below the experimental data while the corresponding estimates within the ACD model may agree with them due to $X(x_t, 1/R) > X_0(x_t)$, see table 4.

Another definite prediction of the ACD model is an *increase* of ΔM_s over the SM value. This should be contrasted with the prediction of the MSSM at large $\tan \beta$ where a *suppression* of ΔM_s with respect to the SM value is predicted [60]. Thus, when the ratio $(\Delta M_s)_{\text{exp}}/(\Delta M_s)_{\text{SM}}$

will be known with a sufficient accuracy, we will know whether the ACD model with a low $1/R$ or the MSSM with a large $\tan\beta$ is ruled out by the data.

A distinction between the ACD model and the MSSM at low $\tan\beta$ will also be possible. In the latter case the supersymmetric effects in $\Delta F = 2$ transitions considered in section 3 are generally larger than in $\Delta F = 1$ transitions so that the branching ratios for $K^+ \rightarrow \pi^+ \nu \bar{\nu}$, $K_L \rightarrow \pi^0 \nu \bar{\nu}$, $K_L \rightarrow \mu^+ \mu^-$, $B \rightarrow X_d \nu \bar{\nu}$ and $B_d \rightarrow \mu \bar{\mu}$ are generally suppressed with respect to the SM while they can be enhanced for special ranges of supersymmetric parameters in the case of $B \rightarrow X_s \nu \bar{\nu}$ and $B_s \rightarrow \mu \bar{\mu}$ [61].

However, the main message from our analysis is the following one. Even for the lowest compactification scale, $1/R = 200$ GeV, considered by us, the ACD model is consistent with all the available data on FCNC processes analyzed here. No fine tuning of the parameters characteristic in the flavour sector for general supersymmetric models is necessary. This is first of all connected with the GIM mechanism that assures the convergence of the sum over the KK modes in the case of Z^0 penguin diagrams, removing the sensitivity of the calculated branching ratios to the scale $M_s \gg 1/R$ at which the higher dimensional theory becomes non-perturbative and at which the towers of the KK particles must be cut off in an appropriate way.

With the much improved data on the processes calculated in this paper and the theoretical uncertainties reduced, it should be possible in the future to distinguish the predictions of the ACD model from the SM ones, provided $1/R < 400$ GeV. For higher compactification scales this distinction will be very difficult with a possible exception of $B_s \rightarrow \mu^+ \mu^-$. Whether these findings apply also to $B \rightarrow X_s \gamma$, $B \rightarrow X_s l^+ l^-$ and $K_L \rightarrow \pi^0 e^+ e^-$ is an interesting question. As the Z^0 -penguins are enhanced in the ACD model, the corresponding enhancement of the branching ratios for $B \rightarrow X_s l^+ l^-$ and $K_L \rightarrow \pi^0 e^+ e^-$ can easily be calculated by means of the known formulae [25, 62, 63]. However, such an analysis would clearly be unsatisfactory as these decays receive also contributions from the γ -penguins and magnetic penguins. The KK contributions to γ -penguins are unknown, while the corresponding contributions to the magnetic penguins have been calculated in the context of an analysis of the decay $B \rightarrow X_s \gamma$ under the assumption of the dominance of the scalars $a_{(n)}^\pm$ [2]. We have seen that this assumption would be correct in the case of $S(x_t, 1/R)$ for $1/R \geq 300$ GeV, but certainly would misrepresent the KK contributions to $C(x_t, 1/R)$ in view of strong cancellations between different contributions as discussed in section 4. Consequently a satisfactory analysis of $B \rightarrow X_s \gamma$, $B \rightarrow X_s l^+ l^-$ and $K_L \rightarrow \pi^0 e^+ e^-$ requires a priori the inclusion of all KK contributions. We will address all these issues in the forthcoming paper [11].

Acknowledgements

We thank Fabrizio Parodi and Achille Stocchi for providing the numbers in the second column of table 1. This research was partially supported by the German ‘Bundesministerium für Bildung und Forschung’ under contract 05HT1WOA3 and by the ‘Deutsche Forschungsgemeinschaft’ (DFG) under contract Bu.706/1-1.

A Feynman Rules in the ACD Model

In this section, we list all propagators and vertex rules needed for the calculation of the box and penguin diagrams considered in this paper. The Feynman rules are derived in the 5d R_ξ -gauge described in Section 2.3.

It is convenient to define a 4 dimensional counterpart to every parameter in the 5 dimensional Lagrangian, marked there with a caret. The conversion factors are chosen in order to eliminate all explicit appearances of factors of $\sqrt{2\pi R}$ in the Feynman rules:

$$\begin{aligned} \mu &= \hat{\mu}, & v &= \sqrt{2\pi R} \hat{v}, & g_2 &= \frac{1}{\sqrt{2\pi R}} \hat{g}_2, \\ g' &= \frac{1}{\sqrt{2\pi R}} \hat{g}', & \lambda_{\mathcal{U}/\mathcal{D}} &= \frac{1}{\sqrt{2\pi R}} \hat{\lambda}_{\mathcal{U}/\mathcal{D}}, \end{aligned} \quad (\text{A.1})$$

where $\hat{\mu}$ is the Higgs mass parameter.

In order to simplify the notation, we omit the KK indices of the fields and of the mass parameters defined in (A.3) and (A.4). There is no ambiguity because in one-loop calculations at least one field is always a zero-mode. In our case, this is the Z boson in the Z vertices, and the down-type quark or the neutrino in all other vertices. Due to KK parity conservation, the other two fields have equal KK mode number, i.e. either zero or $n \geq 1$.

Fermion zero-modes have substantially different Feynman rules than their KK excitations. The fields \mathcal{Q}_u , \mathcal{Q}_d , \mathcal{U} , \mathcal{D} , \mathcal{L}_ν , \mathcal{L}_e and \mathcal{E} are always supposed to be ($n \geq 1$)-modes, while the zero-modes are labeled u , d , ν and e . The generation indices are $i = u, c, t$ and $j = d, s, b$ for the quarks and $i, j = e, \mu, \tau$ for the leptons.

The masses of all bosonic particles can be expressed in terms of four independent mass parameters:

$$\begin{aligned} M_{A(n)}^2 &= \frac{n^2}{R^2}, \\ M_{Z(n)}^2 &= \frac{n^2}{R^2} + M_Z^2, \\ M_{W(n)}^2 &= \frac{n^2}{R^2} + M_W^2, \\ M_{H(n)}^2 &= \frac{n^2}{R^2} + 2\mu^2. \end{aligned} \quad (\text{A.2})$$

We introduce two sets of mass parameters appearing in the fermion-scalar couplings. The

mass parameters $m_x^{(i)}$ are

$$\begin{aligned}
m_1^{(i)} &= \frac{n}{R} c_{i(n)} + m_i s_{i(n)}, \\
m_2^{(i)} &= -\frac{n}{R} s_{i(n)} + m_i c_{i(n)}, \\
m_3^{(i)} &= -M_W c_{i(n)} + \frac{n}{R} \frac{m_i}{M_W} s_{i(n)}, \\
m_4^{(i)} &= M_W s_{i(n)} + \frac{n}{R} \frac{m_i}{M_W} c_{i(n)},
\end{aligned} \tag{A.3}$$

where M_W and the *up-type* fermion masses m_i on the r.h.s. are the zero-mode masses. The parameters $c_{i(n)}$ and $s_{i(n)}$ denote the cosine and sine respectively of the fermion mass mixing angle $\alpha_{i(n)}$ defined in (2.29). The mass parameters $M_x^{(i,j)}$ are

$$\begin{aligned}
M_1^{(i,j)} &= m_j c_{i(n)}, \\
M_2^{(i,j)} &= m_j s_{i(n)}, \\
M_3^{(i,j)} &= \frac{n}{R} \frac{m_j}{M_W} c_{i(n)}, \\
M_4^{(i,j)} &= \frac{n}{R} \frac{m_j}{M_W} s_{i(n)},
\end{aligned} \tag{A.4}$$

where again M_W and the *down-type* fermion masses m_j on the r.h.s. are the zero-mode masses.

All momenta and fields are assumed to be incoming.

A.1 Propagators

The propagators are:

for scalar fields $S = H, a^0, a^\pm, A_5, G^0, G^\pm$:

$S \bullet \text{---} \bullet S$

$$= \frac{i}{k^2 - M^2 + i\epsilon},$$

with the masses

S	$H_{(n)}$	$a_{(n)}^0$	$a_{(n)}^\pm$	$A_{5(n)}$	$G_{(n)}^0$	$G_{(n)}^\pm$
M	$M_{H(n)}$	$M_{Z(n)}$	$M_{W(n)}$	$\sqrt{\xi} M_{A(n)}$	$\sqrt{\xi} M_{Z(n)}$	$\sqrt{\xi} M_{W(n)}$

for gauge bosons $V = A, Z, W^\pm$:

$V_\mu \bullet \text{---} \bullet V_\nu$

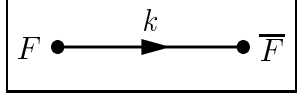
$$= \frac{-i}{k^2 - M^2 + i\epsilon} \left(g^{\mu\nu} - (1 - \xi) \frac{k^\mu k^\nu}{k^2 - \xi M^2 + i\epsilon} \right),$$

with the masses

V	$A_{(n)}$	$Z_{(n)}$	$W_{(n)}^\pm$	
M	$M_{A(n)}$	$M_{Z(n)}$	$M_{W(n)}$	

(A.6)

for fermion fields $F = u, d, \mathcal{Q}_u, \mathcal{Q}_d, \mathcal{U}, \mathcal{D}, \nu, e, \mathcal{L}_\nu, \mathcal{L}_e, \mathcal{E}$:



$$= \frac{i(\not{k} + m)}{k^2 - m^2 + i\epsilon},$$

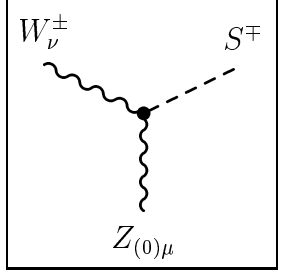
with the masses

F	u	d	$\mathcal{Q}_{u(n)}$	$\mathcal{Q}_{d(n)}$	$\mathcal{U}_{(n)}$	$\mathcal{D}_{(n)}$	ν	e	$\mathcal{L}_{\nu(n)}$	$\mathcal{L}_{e(n)}$	$\mathcal{E}_{(n)}$
m	m_u	m_d	$m_{u(n)}$	$m_{d(n)}$	$m_{u(n)}$	$m_{d(n)}$	m_ν	m_e	$m_{\nu(n)}$	$m_{e(n)}$	$m_{e(n)}$

(A.7)

A.2 Vertices

The Feynman rules for the vertices are:



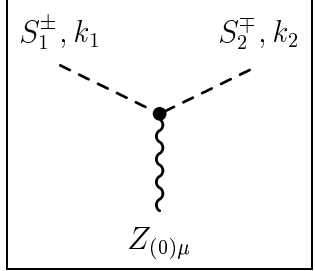
$$= \frac{g_2}{c_w M_{W(n)}} g_{\mu\nu} C.$$

$$ZW^+G^- : \quad C = -s_w^2 M_W^2 + c_w^2 \frac{n^2}{R^2}, \quad (\text{A.8})$$

$$ZW^-G^+ : \quad C = s_w^2 M_W^2 - c_w^2 \frac{n^2}{R^2}, \quad (\text{A.9})$$

$$ZW^+a^- : \quad C = -M_W \frac{n}{R}, \quad (\text{A.10})$$

$$ZW^-a^+ : \quad C = M_W \frac{n}{R}. \quad (\text{A.11})$$



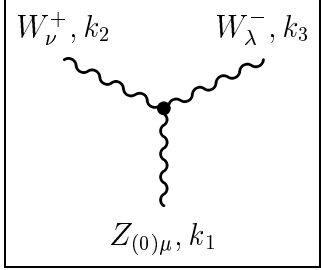
$$= \frac{ig_2}{2c_w M_{W(n)}^2} (k_2 - k_1)_\mu C.$$

$$ZG^+G^- : \quad C = - (c_w^2 - s_w^2) M_W^2 - 2c_w^2 \frac{n^2}{R^2}, \quad (\text{A.12})$$

$$Za^+a^- : \quad C = -2c_w^2 M_W^2 - (c_w^2 - s_w^2) \frac{n^2}{R^2}, \quad (\text{A.13})$$

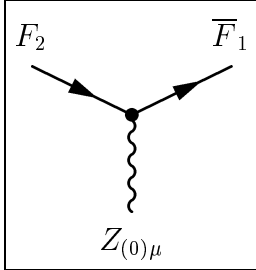
$$ZG^+a^- : \quad C = M_W \frac{n}{R}, \quad (\text{A.14})$$

$$ZG^-a^+ : \quad C = -M_W \frac{n}{R}. \quad (\text{A.15})$$



$$= ig_2 c_w (g_{\mu\nu} (k_2 - k_1)_\lambda + g_{\mu\lambda} (k_1 - k_3)_\nu + g_{\lambda\nu} (k_3 - k_2)_\mu).$$

$$(\text{A.16})$$



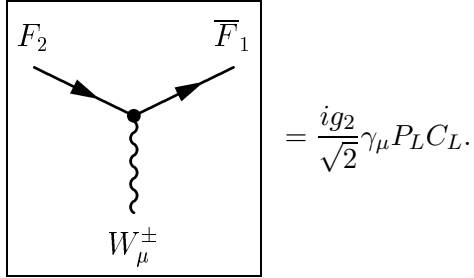
$$= \frac{ig_2}{6c_w} \gamma_\mu (P_L C_L + P_R C_R).$$

$$Z\bar{u}_i u_i : \quad \begin{cases} C_L = 3 - 4s_w^2, \\ C_R = -4s_w^2, \end{cases} \quad Z\bar{d}_j d_j : \quad \begin{cases} C_L = -3 + 2s_w^2, \\ C_R = 2s_w^2, \end{cases} \quad (\text{A.17})$$

$$Z\bar{\nu}_i \nu_i : \quad \begin{cases} C_L = 3, \\ C_R = 0, \end{cases} \quad Z\bar{e}_j e_j : \quad \begin{cases} C_L = -3 + 6s_w^2, \\ C_R = 6s_w^2, \end{cases} \quad (\text{A.18})$$

$$Z\bar{Q}_i Q_i : \quad \begin{cases} C_L = -4s_w^2 + 3c_{i(n)}^2, \\ C_R = -4s_w^2 + 3c_{i(n)}^2, \end{cases} \quad Z\bar{U}_i U_i : \quad \begin{cases} C_L = -4s_w^2 + 3s_{i(n)}^2, \\ C_R = -4s_w^2 + 3s_{i(n)}^2, \end{cases} \quad (\text{A.19})$$

$$Z\bar{Q}_i U_i : \quad \begin{cases} C_L = -3s_{i(n)} c_{i(n)}, \\ C_R = 3s_{i(n)} c_{i(n)}, \end{cases} \quad Z\bar{U}_i Q_i : \quad \begin{cases} C_L = -3s_{i(n)} c_{i(n)}, \\ C_R = 3s_{i(n)} c_{i(n)}. \end{cases} \quad (\text{A.20})$$



$$W^+ \bar{u}_i d_j : \quad C_L = V_{ij}, \quad W^- \bar{d}_j u_i : \quad C_L = V_{ij}^*, \quad (A.21)$$

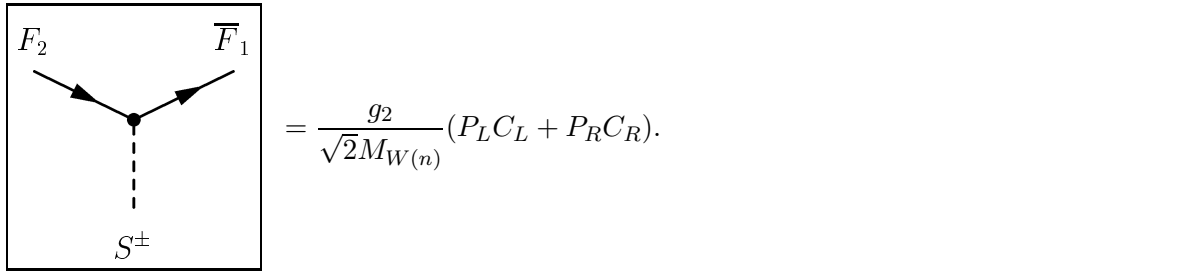
$$W^+ \bar{\mathcal{Q}}_i d_j : \quad C_L = c_{i(n)} V_{ij}, \quad W^- \bar{d}_j \mathcal{Q}_i : \quad C_L = c_{i(n)} V_{ij}^*, \quad (A.22)$$

$$W^+ \bar{\mathcal{U}}_i d_j : \quad C_L = -s_{i(n)} V_{ij}, \quad W^- \bar{d}_j \mathcal{U}_i : \quad C_L = -s_{i(n)} V_{ij}^*, \quad (A.23)$$

$$W^+ \bar{\nu}_i e_j : \quad C_L = \delta_{ij}, \quad W^- \bar{e}_j \nu_i : \quad C_L = \delta_{ij}, \quad (A.24)$$

$$W^+ \bar{\nu}_i \mathcal{L}_j : \quad C_L = \delta_{ij}, \quad W^- \bar{\mathcal{L}}_j \nu_i : \quad C_L = \delta_{ij}, \quad (A.25)$$

$$W^+ \bar{\nu}_i \mathcal{E}_j : \quad C_L = 0, \quad W^- \bar{\mathcal{E}}_j \nu_i : \quad C_L = 0. \quad (A.26)$$



$$G^+ \bar{u}_i d_j : \quad \begin{cases} C_L = -m_i V_{ij}, \\ C_R = m_j V_{ij}, \end{cases} \quad G^- \bar{d}_j u_i : \quad \begin{cases} C_L = -m_j V_{ij}^*, \\ C_R = m_i V_{ij}^*, \end{cases} \quad (A.27)$$

$$G^+ \bar{\mathcal{Q}}_i d_j : \quad \begin{cases} C_L = -m_1^{(i)} V_{ij}, \\ C_R = M_1^{(i,j)} V_{ij}, \end{cases} \quad G^- \bar{d}_j \mathcal{Q}_i : \quad \begin{cases} C_L = -M_1^{(i,j)} V_{ij}^*, \\ C_R = m_1^{(i)} V_{ij}^*, \end{cases} \quad (A.28)$$

$$G^+ \bar{\mathcal{U}}_i d_j : \quad \begin{cases} C_L = m_2^{(i)} V_{ij}, \\ C_R = -M_2^{(i,j)} V_{ij}, \end{cases} \quad G^- \bar{d}_j \mathcal{U}_i : \quad \begin{cases} C_L = M_2^{(i,j)} V_{ij}^*, \\ C_R = -m_2^{(i)} V_{ij}^*, \end{cases} \quad (A.29)$$

$$G^+ \bar{\nu}_i e_j : \quad \begin{cases} C_L = 0, \\ C_R = m_j \delta_{ij}, \end{cases} \quad G^- \bar{e}_j \nu_i : \quad \begin{cases} C_L = -m_j \delta_{ij}, \\ C_R = 0, \end{cases} \quad (A.30)$$

$$G^+ \bar{\nu}_i \mathcal{L}_j : \quad \begin{cases} C_L = 0, \\ C_R = m_1^{(j)} \delta_{ij}, \end{cases} \quad G^- \bar{\mathcal{L}}_j \nu_i : \quad \begin{cases} C_L = -m_1^{(j)} \delta_{ij}, \\ C_R = 0, \end{cases} \quad (A.31)$$

$$G^+ \bar{\nu}_i \mathcal{E}_j : \quad \begin{cases} C_L = 0, \\ C_R = -m_2^{(j)} \delta_{ij}, \end{cases} \quad G^- \bar{\mathcal{E}}_j \nu_i : \quad \begin{cases} C_L = m_2^{(j)} \delta_{ij}, \\ C_R = 0, \end{cases} \quad (A.32)$$

$$a^+ \overline{\mathcal{Q}}_i d_j : \begin{cases} C_L = -m_3^{(i)} V_{ij}, \\ C_R = M_3^{(i,j)} V_{ij}, \end{cases} \quad a^- \overline{d}_j \mathcal{Q}_i : \begin{cases} C_L = -M_3^{(i,j)} V_{ij}^*, \\ C_R = m_3^{(i)} V_{ij}^*, \end{cases} \quad (\text{A.33})$$

$$a^+ \overline{\mathcal{U}}_i d_j : \begin{cases} C_L = m_4^{(i)} V_{ij}, \\ C_R = -M_4^{(i,j)} V_{ij}, \end{cases} \quad a^- \overline{d}_j \mathcal{U}_i : \begin{cases} C_L = M_4^{(i,j)} V_{ij}^*, \\ C_R = -m_4^{(i)} V_{ij}^*, \end{cases} \quad (\text{A.34})$$

$$a^+ \overline{\nu}_i \mathcal{L}_j : \begin{cases} C_L = 0, \\ C_R = m_3^{(j)} \delta_{ij}, \end{cases} \quad a^- \overline{\mathcal{L}}_j \nu_i : \begin{cases} C_L = -m_3^{(j)} \delta_{ij}, \\ C_R = 0, \end{cases} \quad (\text{A.35})$$

$$a^+ \overline{\nu}_i \mathcal{E}_j : \begin{cases} C_L = 0, \\ C_R = -m_4^{(j)} \delta_{ij}, \end{cases} \quad a^- \overline{\mathcal{E}}_j \nu_i : \begin{cases} C_L = m_4^{(j)} \delta_{ij}, \\ C_R = 0. \end{cases} \quad (\text{A.36})$$

B Different Contributions to $\Delta F = 2$ Box Diagrams

The contributions from different sets of diagrams to the functions $F(x_{t(n)}, x_{u(n)})$ in (3.8) are given as follows

$$F_{WW(n)} = \frac{M_W^2}{M_{W(n)}^2} U(x_{t(n)}, x_{u(n)}), \quad (\text{B.1})$$

$$F_{WG(n)} = -2 \frac{M_W^2 m_{t(n)} m_{u(n)}}{M_{W(n)}^6} \left[m_1^{(t)} c_{t(n)} + m_2^{(t)} s_{t(n)} \right] \left[m_1^{(u)} c_{u(n)} + m_2^{(u)} s_{u(n)} \right] \times \tilde{U}(x_{t(n)}, x_{u(n)}), \quad (\text{B.2})$$

$$F_{Wa(n)} = -2 \frac{M_W^2 m_{t(n)} m_{u(n)}}{M_{W(n)}^6} \left[m_3^{(t)} c_{t(n)} + m_4^{(t)} s_{t(n)} \right] \left[m_3^{(u)} c_{u(n)} + m_4^{(u)} s_{u(n)} \right] \times \tilde{U}(x_{t(n)}, x_{u(n)}), \quad (\text{B.3})$$

$$F_{Ga(n)} = \frac{1}{2} \frac{M_W^2}{M_{W(n)}^6} \left[m_1^{(t)} m_3^{(t)} + m_2^{(t)} m_4^{(t)} \right] \left[m_1^{(u)} m_3^{(u)} + m_2^{(u)} m_4^{(u)} \right] \times U(x_{t(n)}, x_{u(n)}), \quad (\text{B.4})$$

$$F_{GG(n)} = \frac{1}{4} \frac{M_W^2}{M_{W(n)}^6} \left[(m_1^{(t)})^2 + (m_2^{(t)})^2 \right] \left[(m_1^{(u)})^2 + (m_2^{(u)})^2 \right] U(x_{t(n)}, x_{u(n)}), \quad (\text{B.5})$$

$$F_{aa(n)} = \frac{1}{4} \frac{M_W^2}{M_{W(n)}^6} \left[(m_3^{(t)})^2 + (m_4^{(t)})^2 \right] \left[(m_3^{(u)})^2 + (m_4^{(u)})^2 \right] U(x_{t(n)}, x_{u(n)}). \quad (\text{B.6})$$

The functions U and \tilde{U} are defined as follows

$$U(x_t, x_u) = \frac{x_t^2 \log x_t}{(x_t - x_u)(1 - x_t)^2} + \frac{x_u^2 \log x_u}{(x_u - x_t)(1 - x_u)^2} + \frac{1}{(1 - x_u)(1 - x_t)}, \quad (\text{B.7})$$

$$U(x_t, x_t) = \frac{2x_t \log x_t}{(1 - x_t)^3} + \frac{1 + x_t}{(1 - x_t)^2}, \quad (\text{B.8})$$

$$\tilde{U}(x_t, x_u) = \frac{x_t \log x_t}{(x_t - x_u)(1 - x_t)^2} + \frac{x_u \log x_u}{(x_u - x_t)(1 - x_u)^2} + \frac{1}{(1 - x_u)(1 - x_t)}, \quad (\text{B.9})$$

$$\tilde{U}(x_t, x_t) = \frac{(1 + x_t) \log x_t}{(1 - x_t)^3} + \frac{2}{(1 - x_t)^2}. \quad (\text{B.10})$$

C Different Contributions to Z^0 -Penguin Diagrams

The contributions of the diagrams in fig. 6 to the functions $F(x_f)$ in (4.12) are given as follows

$$\begin{aligned} F_1(x_{f(n)}) &= \frac{1}{8} \left(c_{f(n)}^4 + s_{f(n)}^4 - \frac{4}{3} s_w^2 \right) \\ &\quad \times \left[\Delta + \ln \frac{\mu^2}{m_{f(n)}^2} + h_q(x_{f(n)}) - \frac{3}{2} - 2x_{f(n)}h_q(x_{f(n)}) \right], \end{aligned} \quad (\text{C.1})$$

$$F_2(x_{f(n)}) = \frac{1}{4} c_{f(n)}^2 s_{f(n)}^2 \left[\Delta + \ln \frac{\mu^2}{m_{f(n)}^2} - \frac{3}{2} + h_q(x_{f(n)}) + 2x_{f(n)}h_q(x_{f(n)}) \right], \quad (\text{C.2})$$

$$\begin{aligned} F_3(x_{f(n)}) &= \frac{1}{16m_{W(n)}^2} \left[\left((m_1^{(f)})^2 + (m_3^{(f)})^2 \right) \left(c_{f(n)}^2 - \frac{4}{3} s_w^2 \right) + \left((m_2^{(f)})^2 + (m_4^{(f)})^2 \right) \left(s_{f(n)}^2 - \frac{4}{3} s_w^2 \right) \right] \\ &\quad \times \left[\Delta + \ln \frac{\mu^2}{m_{f(n)}^2} - \frac{1}{2} + h_q(x_{f(n)}) - 2x_{f(n)}h_q(x_{f(n)}) \right], \end{aligned} \quad (\text{C.3})$$

$$\begin{aligned} F_4(x_{f(n)}) &= -\frac{1}{8M_{W(n)}^2} \left(m_1^{(f)} m_2^{(f)} + m_3^{(f)} m_4^{(f)} \right) c_{f(n)} s_{f(n)} \\ &\quad \times \left[\Delta + \ln \frac{\mu^2}{m_{f(n)}^2} - \frac{1}{2} + h_q(x_{f(n)}) + 2x_{f(n)}h_q(x_{f(n)}) \right], \end{aligned} \quad (\text{C.4})$$

$$F_5(x_{f(n)}) = -\frac{3}{4} c_w^2 \left[\Delta + \ln \frac{\mu^2}{M_{W(n)}^2} - \frac{1}{6} - x_{f(n)}h_w(x_{f(n)}) \right], \quad (\text{C.5})$$

$$\begin{aligned} F_6(x_{f(n)}) &= -\frac{1}{16m_{W(n)}^4} \left[\left((1 - 2s_w^2) M_W^2 + 2c_w^2 \frac{n^2}{R^2} \right) \left((m_1^{(f)})^2 + (m_2^{(f)})^2 \right) \right. \\ &\quad \left. + \left((1 - 2s_w^2) \frac{n^2}{R^2} + 2c_w^2 M_W^2 \right) \left((m_3^{(f)})^2 + (m_4^{(f)})^2 \right) \right] \\ &\quad \times \left[\Delta + \ln \frac{\mu^2}{M_{W(n)}^2} + \frac{1}{2} - x_{f(n)}h_w(x_{f(n)}) \right], \end{aligned} \quad (\text{C.6})$$

$$\begin{aligned}
F_7(x_{f(n)}) &= \frac{M_W}{8M_{W(n)}^4} \frac{n}{R} \left(m_1^{(f)} m_3^{(f)} + m_2^{(f)} m_4^{(f)} \right) \\
&\quad \times \left[\Delta + \ln \frac{\mu^2}{M_{W(n)}^2} + \frac{1}{2} - x_{f(n)} h_w(x_{f(n)}) \right], \tag{C.7}
\end{aligned}$$

$$\begin{aligned}
F_8(x_{f(n)}) &= \frac{m_{f(n)}}{2M_{W(n)}^4} \left[\left(s_w^2 M_W^2 - c_w^2 \frac{n^2}{R^2} \right) \left(m_1^{(f)} c_{f(n)} + m_2^{(f)} s_{f(n)} \right) \right. \\
&\quad \left. + M_W \frac{n}{R} \left(m_3^{(f)} c_{f(n)} + m_4^{(f)} s_{f(n)} \right) \right] h_w(x_{f(n)}). \tag{C.8}
\end{aligned}$$

Here

$$\Delta = \frac{1}{\epsilon} + \ln 4\pi - \gamma_E, \quad D = 4 - 2\epsilon \tag{C.9}$$

and the functions h_q and h_w are given by:

$$h_q(x) = \frac{1}{1-x} + \frac{\ln x}{(1-x)^2}, \tag{C.10}$$

$$h_w(x) = \frac{1}{1-x} + \frac{x \ln x}{(1-x)^2}. \tag{C.11}$$

Finally, the contributions from counter terms corresponding to the self-energy diagrams of fig. 11 that should be added to the functions F_i are given by

$$\Delta S_1(x_{f(n)}) = \frac{1}{4} \left(\Delta - \frac{1}{2} \left(\frac{1+x_{f(n)}}{1-x_{f(n)}} + \frac{2x_{f(n)}^2 \ln x_{f(n)}}{(1-x_{f(n)})^2} \right) - \ln \frac{M_{W(n)}^2}{\mu^2} \right), \tag{C.12}$$

$$\Delta S_2(x_{f(n)}) = \frac{1}{8} (1+x_f) \left(\Delta + \frac{1}{2} \left(\frac{1-3x_{f(n)}}{1-x_{f(n)}} - \frac{2x_{f(n)}^2 \ln x_{f(n)}}{(1-x_{f(n)})^2} \right) - \ln \frac{M_{W(n)}^2}{\mu^2} \right). \tag{C.13}$$

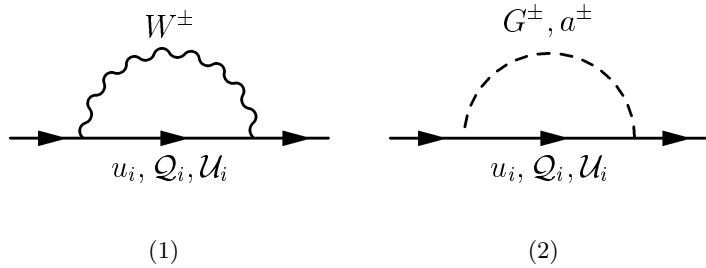


Figure 11: Self-energy diagrams necessary for calculating the electroweak counter term as discussed in [50].

D Different Contributions to $\Delta F = 1$ Box Diagrams

The one loop amplitude of the KK excitations in the diagrams in fig. 8 is a sum of contributions coming from the various bosonic fields in the loop

$$G_n(x_{f(n)}, x_{e(n)}) = G_{WW(n)} + G_{WG(n)} + G_{Wa(n)} + G_{Ga(n)} + G_{GG(n)} + G_{aa(n)}, \quad (\text{D.1})$$

$$H_n(x_{f(n)}, x_{\nu(n)}) = H_{WW(n)} + H_{WG(n)} + H_{Wa(n)} + H_{Ga(n)} + H_{GG(n)} + H_{aa(n)}. \quad (\text{D.2})$$

The explicit results for $B_n^{\nu\bar{\nu}}(x_t, x_n)$ and $B_n^{\mu\bar{\mu}}(x_t, x_n)$ are given by

$$\begin{aligned} B_n^{\nu\bar{\nu}}(x_t, x_n) &= G_n(x_{t(n)}, x_{e(n)}) - G_n(x_{u(n)}, x_{e(n)}), \\ B_n^{\mu\bar{\mu}}(x_t, x_n) &= H_n(x_{t(n)}, x_{\nu(n)}) - H_n(x_{u(n)}, x_{\nu(n)}), \end{aligned} \quad (\text{D.3})$$

where the results for the $\nu\bar{\nu}$ -box diagrams take the form

$$G_{WW(n)} = -\frac{M_W^2}{M_{W(n)}^2} U(x_{f(n)}, x_{e(n)}), \quad (\text{D.4})$$

$$G_{WG(n)} = \frac{1}{2} \frac{M_W^2 m_{f(n)} m_{e(n)}}{M_{W(n)}^6} \left[m_1^{(f)} c_{f(n)} + m_2^{(f)} s_{f(n)} \right] m_1^{(e)} \tilde{U}(x_{f(n)}, x_{e(n)}), \quad (\text{D.5})$$

$$G_{Wa(n)} = \frac{1}{2} \frac{M_W^2 m_{f(n)} m_{e(n)}}{M_{W(n)}^6} \left[m_3^{(f)} c_{f(n)} + m_4^{(f)} s_{f(n)} \right] m_3^{(e)} \tilde{U}(x_{f(n)}, x_{e(n)}), \quad (\text{D.6})$$

$$G_{Ga(n)} = -\frac{1}{8} \frac{M_W^2}{M_{W(n)}^6} \left[m_1^{(f)} m_3^{(f)} + m_2^{(f)} m_4^{(f)} \right] m_1^{(e)} m_3^{(e)} U(x_{f(n)}, x_{e(n)}), \quad (\text{D.7})$$

$$G_{GG(n)} = -\frac{1}{16} \frac{M_W^2}{M_{W(n)}^6} \left[(m_1^{(f)})^2 + (m_2^{(f)})^2 \right] (m_1^{(e)})^2 U(x_{f(n)}, x_{e(n)}), \quad (\text{D.8})$$

$$G_{aa(n)} = -\frac{1}{16} \frac{M_W^2}{M_{W(n)}^6} \left[(m_3^{(f)})^2 + (m_4^{(f)})^2 \right] (m_3^{(e)})^2 U(x_{f(n)}, x_{e(n)}), \quad (\text{D.9})$$

and for the $\mu\bar{\mu}$ -box diagrams we get

$$H_{WW(n)} = -\frac{1}{4} \frac{M_W^2}{M_{W(n)}^2} U(x_{f(n)}, x_{\nu(n)}), \quad (\text{D.10})$$

$$H_{WG(n)} = \frac{1}{2} \frac{M_W^2 m_{f(n)} m_{\nu(n)}}{M_{W(n)}^6} \left[m_1^{(f)} c_{f(n)} + m_2^{(f)} s_{f(n)} \right] m_1^{(\nu)} \tilde{U}(x_{f(n)}, x_{\nu(n)}), \quad (\text{D.11})$$

$$H_{Wa(n)} = \frac{1}{2} \frac{M_W^2 m_{f(n)} m_{\nu(n)}}{M_{W(n)}^6} \left[m_3^{(f)} c_{f(n)} + m_4^{(f)} s_{f(n)} \right] m_3^{(\nu)} \tilde{U}(x_{f(n)}, x_{\nu(n)}), \quad (\text{D.12})$$

$$H_{Ga(n)} = -\frac{1}{8} \frac{M_W^2}{M_{W(n)}^6} \left[m_1^{(t)} m_3^{(f)} + m_2^{(f)} m_4^{(f)} \right] m_1^{(\nu)} m_3^{(\nu)} U(x_{f(n)}, x_{\nu(n)}), \quad (\text{D.13})$$

$$H_{GG(n)} = -\frac{1}{16} \frac{M_W^2}{M_{W(n)}^6} \left[(m_1^{(f)})^2 + (m_2^{(f)})^2 \right] (m_1^{(\nu)})^2 U(x_{f(n)}, x_{\nu(n)}), \quad (\text{D.14})$$

$$H_{aa(n)} = -\frac{1}{16} \frac{M_W^2}{M_{W(n)}^6} \left[(m_3^{(f)})^2 + (m_4^{(f)})^2 \right] (m_3^{(\nu)})^2 U(x_{f(n)}, x_{\nu(n)}). \quad (\text{D.15})$$

The functions U and \tilde{U} are defined in (B.7)–(B.10). We have taken into account the overall minus sign in (4.8).

Summing all the contributions we find

$$\begin{aligned} B_n^{\nu\bar{\nu}}(x_t, x_n) &= \frac{17x_t + 18x_n x_t - 9x_n}{16(x_t - 1)} + \frac{x_n(26x_t + 9x_n + 18x_n x_t)}{16x_t} \ln \frac{x_n}{1+x_n} \\ &\quad - \frac{(x_n + x_t)(9x_n + 17x_t)}{16(x_t - 1)^2 x_t} \ln \frac{x_n + x_t}{1+x_n}, \end{aligned} \quad (\text{D.16})$$

$$\begin{aligned} B_n^{\mu\bar{\mu}}(x_t, x_n) &= \frac{3x_n + 5x_t - 6x_n x_t}{16(x_t - 1)} - \frac{x_n(3x_n + 6x_n x_t - 2x_t)}{16x_t} \ln \frac{x_n}{1+x_n} \\ &\quad + \frac{(3x_n - 5x_t)(x_n + x_t)}{16(x_t - 1)^2 x_t} \ln \frac{x_n + x_t}{1+x_n}. \end{aligned} \quad (\text{D.17})$$

References

- [1] T. Appelquist, H.-C. Cheng and B. A. Dobrescu, Phys. Rev. **D64** (2001) 035002, [arXiv:hep-ph/0012100].
- [2] K. Agashe, N. G. Deshpande and G. H. Wu, Phys. Lett. B **514** (2001) 309, [arXiv:hep-ph/0105084].
- [3] K. Agashe, N. G. Deshpande and G. H. Wu, Phys. Lett. B **511** (2001) 85, [arXiv:hep-ph/0103235]; T. Appelquist and B. A. Dobrescu, Phys. Lett. B **516** (2001) 85, [arXiv:hep-ph/0106140].
- [4] C. Macesanu, C.D. McMullen and S. Nandi, Phys. Rev. D **66** (2002) 015009 [arXiv:hep-ph/0201300].
- [5] H. C. Cheng, K. T. Matchev and M. Schmaltz, Phys. Rev. D **66** (2002) 056006 [arXiv:hep-ph/0205314].
- [6] T. G. Rizzo, Phys. Rev. D **64** (2001) 095010 [arXiv:hep-ph/0106336].
- [7] F. J. Petriello, JHEP **0205** (2002) 003 [arXiv:hep-ph/0204067].
- [8] G. Servant and T. M. Tait, [arXiv:hep-ph/0206071].
- [9] H. C. Cheng, J. L. Feng and K. T. Matchev, [arXiv:hep-ph/0207125]; D. Hooper and G. D. Kribs, [arXiv:hep-ph/0208261]; G. Servant and T. M. Tait, [arXiv:hep-ph/0209262]; D. Majumdar, [arXiv:hep-ph/0209277].
- [10] T. Appelquist and H. Yee, [arXiv:hep-ph/0211023].
- [11] A.J. Buras, A. Poschenrieder, M. Spranger and A. Weiler, in preparation.
- [12] S.L. Glashow, J. Iliopoulos and L. Maiani Phys. Rev. **D 2** (1970) 1285.
- [13] J. Papavassiliou and A. Santamaria, Phys. Rev. **D 63** (2001) 016002. J.F. Oliver, J. Papavassiliou and A. Santamaria, [arXiv:hep-ph/0209021].
- [14] A.J. Buras, P. Gambino, M. Gorbahn, S. Jäger and L. Silvestrini, Phys. Lett. **B500** (2001) 161.
- [15] T. Inami and C.S. Lim, Progr. Theor. Phys. **65** (1981) 297.
- [16] A.J. Buras, W. Slominski and H. Steger, Nucl. Phys. **B238** (1984) 529, Nucl. Phys. **B245** (1984) 369.

- [17] G. Buchalla, A.J. Buras and M.K. Harlander, Nucl. Phys. **B** **349** (1991) 1.
- [18] D. Chakraverty, K. Huitu and A. Kundu, [arXiv:hep-ph/0212047].
- [19] A. Muck, A. Pilaftsis and R. Ruckl, [arXiv:hep-ph/0210410]; A. Muck, A. Pilaftsis and R. Ruckl, [arXiv:hep-ph/0209371]; A. Muck, A. Pilaftsis and R. Ruckl, [arXiv:hep-ph/0203032]; A. Muck, A. Pilaftsis and R. Ruckl, Phys. Rev. D **65** (2002) 085037, [arXiv:hep-ph/0110391].
- [20] H. Georgi, A. K. Grant and G. Hailu, Phys. Rev. D **63** (2001) 064027, [arXiv:hep-ph/0007350].
- [21] J. Giedt, [arXiv:hep-ph/0204315].
- [22] H. C. Cheng, K. T. Matchev and M. Schmaltz, Phys. Rev. D **66** (2002) 036005 [arXiv:hep-ph/0204342].
- [23] A.J. Buras, M. Jamin, and P.H. Weisz, Nucl. Phys. **B347** (1990) 491.
- [24] J. Urban, F. Krauss, U. Jentschura and G. Soff, Nucl. Phys. **B523** (1998) 40.
- [25] A.J. Buras, lectures at the International Erice School, August, 2000, [arXiv:hep-ph/0101336].
- [26] K.R. Dienes, E. Dudas and T. Gherghetta, Nucl. Phys. **B537** (1999) 47.
- [27] S. Herrlich and U. Nierste, Nucl. Phys. **B419** (1994) 292 and U. Nierste, recent update.
- [28] S. Herrlich and U. Nierste, Phys. Rev. **D52** (1995) 6505; Nucl. Phys. **B476** (1996) 27.
- [29] L. Wolfenstein, Phys. Rev. Lett. **51** (1983) 1945.
- [30] A.J. Buras, M.E. Lautenbacher and G. Ostermaier, Phys. Rev. **D** **50** (1994) 3433.
- [31] LEP Working group on oscillations :
http://lepbosc.web.cern.ch/LEPBOSC/combined_results/amsterdam_2002/
- [32] L. Lellouch, [arXiv:hep-ph/0211359]; D. Becirevic, [arXiv:hep-ph/0211340].
- [33] A.A. Penin and M. Steinhauser, Phys. Rev. **D65** (2002) 054006; M. Jamin and B.O. Lange, Phys. Rev. **D65** (2002) 056005; K. Hagiwara, S. Narison and D. Nomura, [arXiv:hep-ph/0205092].
- [34] A.J. Buras, F. Parodi and A. Stocchi, [arXiv:hep-ph/0207101].

- [35] B. Aubert et al., BaBar Collaboration, [arXiv:hep-ex/0207042].
- [36] K. Abe et al., Belle Collaboration, [arXiv:hep-ex/0208025].
- [37] Y. Nir, [arXiv:hep-ph/0110278].
- [38] G. D'Ambrosio, G.F. Giudice, G. Isidori and A. Strumia, [arXiv:hep-ph/0207036].
- [39] M. Ciuchini, G. D'Agostini, E. Franco, V. Lubicz, G. Martinelli, F. Parodi, P. Roudeau, A. Stocchi, JHEP 0107(2001) 013, [arXiv:hep-ph/0012308].
- [40] A. Stocchi, [arXiv:hep-ph/0211245].
- [41] A.J. Buras, [arXiv:hep-ph/0210291] and references therein.
- [42] A. Höcker, H. Lacker, S. Laplace and F. Le Diberder, Eur. Phys. J. **C21** (2001) 225 and <http://ckmfitter.in2p3.fr>.
- [43] Provided by F. Parodi and A. Stocchi.
- [44] G. Buchalla and A.J. Buras, Phys. Lett. **B333** (1994) 221, Phys. Rev. **D54** (1996) 6782.
- [45] Y. Grossman and Y. Nir, Phys. Lett. **B398** (1997) 163.
- [46] G. Buchalla and A.J. Buras, Nucl. Phys. **B 400** (1993) 225.
- [47] M. Misiak and J. Urban, Phys. Lett. **B541** (1999) 161.
- [48] G. Buchalla and A.J. Buras, Nucl. Phys. **B 548** (1999) 309.
- [49] G. Buchalla and A.J. Buras, Nucl. Phys. **B 412** (1994) 106.
- [50] G. Buchalla and A.J. Buras, Nucl. Phys. **B 398** (1993) 285.
- [51] K. Hagiwara et al., “Review of Particle Physics”, Phys. Rev. **D 66** (2002) 010001.
- [52] W. Marciano and Z. Parsa, Phys. Rev. **D53**, R1 (1996).
- [53] N. Cabibbo and L. Maiani, Phys. Lett. **B79** (1978) 109.
- [54] C.S. Kim and A.D. Martin, Phys. Lett. **B225** (1989) 186.
- [55] G. D'Ambrosio, G. Isidori and J. Portolés, Phys. Lett. **423** (1998) 385; G. Isidori and A. Retico, JHEP **0209** (2002) 063.

- [56] S. Adler et al., Phys. Rev. Lett. **79**, (1997) 2204, Phys. Rev. Lett. **84**, (2000) 3768, [arXiv:hep-ex/0111091].
- [57] G. D'Ambrosio and G. Isidori, [arXiv:hep-ph/0112135].
- [58] D. Becirevic, S. Fajfer, S. Prelovsek and J. Zupan, [arXiv:hep-ph/0211271].
- [59] A.J. Buras and R. Fleischer, Phys. Rev. **D64** (2001) 115010. A.J. Buras and R. Buras, Phys. Lett. **501** (2001) 223. S. Bergmann and G. Perez, Phys. Rev. **D64** (2001) 115009, JHEP **0008** (2000) 034. S. Laplace, Z. Ligeti, Y. Nir and G. Perez, Phys. Rev. **D65** (2002) 094040.
- [60] A.J. Buras, P.H. Chankowski, J. Rosiek and L. Sławianowska, Nucl. Phys. **B619** (2001) 434, Phys. Lett. **546** (2002) 96, [arXiv:hep-ph/0210145].
- [61] A.J. Buras, P. Gambino, M. Gorbahn, S. Jäger and L. Silvestrini, Nucl. Phys. **B592** (2001) 55.
- [62] A.J. Buras and L. Silvestrini, Nucl. Phys. **B** **546** (1999) 299.
- [63] G. Buchalla, G. Hiller and G. Isidori, Phys. Rev. **D63** (2001) 014015.